JCB Journal of Cell Biology

ARTICLE

WDR91 specifies the endosomal retrieval subdomain for retromer-dependent recycling

Nan Liu[1], Kai Liu[1], and Chonglin Yang[1]

Retromer-dependent endosomal recycling of membrane receptors requires Rab7, sorting nexin (SNX)-retromer, and factors that regulate endosomal actin organization. It is not fully understood how these factors cooperate to form endosomal subdomains for cargo retrieval and recycling. Here, we report that WDR91, a Rab7 effector, is the key factor that specifies the endosomal retrieval subdomain. Loss of WDR91 causes defective recycling of both intracellular and cell surface receptors. WDR91 interacts with SNXs through their PX domain, and with VPS35, thus promoting their interaction with Rab7. WDR91 also interacts with the WASH subunit FAM21. In WDR91-deficient cells, Rab7, SNX-retromer, and FAM21 fail to localize to endosomal subdomains, and endosomal actin organization is impaired. Re-expression of WDR91 enables Rab7, SNX-retromer, and FAM21 to concentrate at WDR91-specific endosomal subdomains, where retromer-mediated membrane tubulation and release occur. Thus, WDR91 coordinates Rab7 with SNX-retromer and WASH to establish the endosomal retrieval subdomains required for retromer-mediated endosomal recycling.

Introduction

The retromer complex plays a pivotal role in endosomal retrieval and recycling of transmembrane proteins, including plasma membrane receptors and intracellular receptors (Burd and Cullen, 2014; Cullen and Steinberg, 2018). In yeast, retromer comprises two subcomplexes, the cargo-selective Vps26-Vps29-Vps35 trimer and the PtdIns3P-binding and membrane-deforming Vps5-Vps17 heterodimer (Seaman et al., 1998). In mammalian cells, retromer usually refers to the stable cargo-selecting VPS26-VPS29-VPS35 complex (CSC), which acts in combination with distinct sorting nexins (SNXs). While SNXs contain a PtdIns3P-binding PX (Phox homology) domain for recruitment to early endosomes, CSC on its own does not bind to endosomal membranes. Instead, it is recruited to the endosome by interacting with the active GTP-bound Rab7 and SNX3 (Harrison et al., 2014; Harterink et al., 2011; Rojas et al., 2008; Seaman et al., 2009). Retromer/CSC interacts with distinct combinations of SNXs to mediate cargo-specific retrieval and recycling from endosomes (Cullen and Korswagen, 2011). The SNX-BAR-retromer consists of CSC and a heterodimer of SNX1 or SNX2 with SNX5 or SNX6, which are homologous to yeast Vps5-Vps17 and contain a PX domain and a membrane-deforming BAR (Bin-Amphiphysin-Rvs) domain. SNX-BAR-retromer mediates retrograde trafficking from endosomes to the trans Golgi network (TGN). The SNX3-retromer, composed of CSC and the non-BAR domain-containing SNX3, is responsible for endosome-to-TGN recycling of the Wnt receptor Wntless (Harterink et al., 2011). The SNX27-retromer mediates the recycling of membrane receptors from the endosome to the plasma membrane (Lauffer et al., 2010; Temkin et al., 2011). SNX27 contains a PDZ (PSD95/Dlg/ZO) domain, a PX domain, and a FERM (4.1/Ezrin/Radixin/Moesin-like) domain, which serves as a cargo adaptor by interacting with a wide variety of plasma membrane proteins (Steinberg et al., 2013). Within the retromer, VPS35 binds with the FAM21 subunit of the pentameric WASH (Wiskott–Aldrich Syndrome protein and SCAR Homolog) complex, thereby recruiting the latter to the endosome (Harbour et al., 2012; Jia et al., 2012). Endosomal WASH in turn promotes Arp2/3 (actin-related protein 2/3)-dependent actin nucleation and polymerization of branched actin filaments (Derivery et al., 2009; Gomez and Billadeau, 2009). These processes mediate formation and stabilization of endosomal retrieval subdomains, from which retromer-mediated cargo retrieval and subsequent recycling take place (McNally and Cullen, 2018; Norris and Grant, 2020; Puthenveedu et al., 2010; Simonetti and Cullen, 2019).

Retromer-mediated endosomal cargo recycling is intrinsically coupled to early-to-late endosome conversion along the endosome–lysosome pathway. Endosome conversion is characterized by the switching of early endosome-specific Rab5 and PtdIns3P to late endosome-specific Rab7 and PtdIns(3,5)P_2

[1]State Key Laboratory of Conservation and Utilization of Bio-resources in Yunnan, Center for Life Sciences, School of Life Sciences, Yunnan University, Kunming, China.

Correspondence to Chonglin Yang: clyang@ynu.edu.cn.

(Huotari and Helenius, 2011; Rink et al., 2005). Rab5 interacts with VPS34 to promote the generation of endosomal PtdIns3P, which is important for association of SNXs with early endosomes. Upon the conversion of endosomes, the decrease of PtdIns3P probably weakens the association of SNXs with endosomes (Burda et al., 2002; Carlton et al., 2005; Cozier et al., 2002; Teasdale and Collins, 2012; Xu et al., 2001; Zhong et al., 2002). Endosomal switching of Rab5 to Rab7 leads to the interaction of Rab7 with CSC and hence to endosomal recruitment of CSC (Rojas et al., 2008; Seaman et al., 2009). SNX-retromer then facilitates membrane tubulation from Rab7-enriched subdomains (Rojas et al., 2008; van Weering et al., 2012). The requirement for Rab7 in SNX-retromer–mediated endosomal recycling is further evidenced by the finding that TBC1D5, a Rab7 GTPase-activating protein that interacts with VPS29, inhibits endosomal association of the CSC complex (Jia et al., 2016; Seaman et al., 2009). However, it is currently not understood how Rab7 coordinates CSC and the PtdIns3P-binding SNXs for retrieval and recycling of endosomal cargos. In addition, given that retromer acts as a Rab7 effector (Nakada-Tsukui et al., 2005; Rojas et al., 2008; Seaman et al., 2009), it is not known whether additional Rab7 effectors participate directly in Rab7-dependent retromer recycling.

Among the many Rab7 effectors, the WD40 repeat-containing protein WDR91 plays multiple roles in the endosome–lysosome pathway. WDR91 is recruited to the endosome by the active GTP-bound Rab7 (GTP-Rab7), which couples PtdIns3P downregulation with Rab switching for early-to-late endosome conversion (Liu et al., 2016; Liu et al., 2017). In addition, WDR91 competes against the HOPS (homotypic fusion and protein sorting) component VPS41 for binding to Rab7 and thus maintains appropriate fusion of late endosomes/lysosomes (Xing et al., 2021). In this study, we reveal that WDR91 is required for endosomal recycling of membrane receptors. Loss of WDR91 strongly inhibits the formation of endosomal retrieval subdomains. At the molecular level, we show that WDR91 promotes the interaction of Rab7 with SNXs and VPS35, which restricts Rab7 and SNX-retromer for formation of retrieval subdomains on the endosome. Our findings demonstrate that WDR91 specifies the endosomal retrieval subdomain, which is indispensable for retromer-dependent recycling of endosomal cargoes.

Results

Loss of WDR91 causes defective recycling of membrane receptors

To investigate whether WDR91 participates in endosomal recycling of membrane receptors, we first examined the internalization and subsequent recycling back to the cell surface of the AMPA receptor GluA2 in mouse primary hippocampal neurons. GluA2 was fused at the extracellular N-terminus with a pH-sensitive GFP variant, pHluorin (pH-GluA2; Fig. 1 A). pH-GluA2 displays green fluorescence at the cell surface but exhibits strongly reduced signals when endocytosed to endosomes with intraluminal pH < 6.0. This allows time-course chasing of GluA2 internalization and recycling between the plasma membrane and endosomes (Ashby et al., 2004; Lin and Huganir, 2007). As expected, surface-localized pH-GluA2 displayed green fluorescence in both wild-type (*Wdr91*$^{+/+}$) and *Wdr91*$^{-/-}$ mouse hippocampal neurons. Upon stimulation by glutamate, a rapid decline in pH-GluA2 fluorescence signals was observed in both groups, indicating that glutamate induced the internalization of pH-GluA2 to endosomes (Fig. 1 B). Following the removal of glutamate, however, the recovery of pH-GluA2 fluorescence in *Wdr91*$^{-/-}$ neurons was much slower than in the wild-type neurons (Fig. 1, B–D). This suggests that loss of WDR91 impaired the recycling of AMPA receptor back to the neuronal cell surface. Next, we examined the endosomal trafficking of β_2-adrenergic receptor (β_2AR) tagged with Flag at the extracellular N-terminus in HeLa cells (Fig. 1 E). In both control (Ctrl) and *WDR91* knockout (KO-91) HeLa cells, Flag-β_2AR localized to the plasma membrane and was induced by isoproterenol, an adrenergic agonist, to localize to endosomes positive for the early endosomal protein EEA1 (Fig. 1 F; Lauffer et al., 2010; Temkin et al., 2011). In KO-91 cells, the endosomes were enlarged, as reported previously (Liu et al., 2016; Liu et al., 2017). Following removal of isoproterenol, Flag-β_2AR re-appeared on the plasma membrane in Ctrl HeLa cells within 30 min (Fig. 1 F). In contrast, the majority of Flag-β_2AR remained on EEA1-endosomes in KO-91 cells at the same time points (Fig. 1, F and G). The time required for Flag-β_2AR to fully return to the plasma membrane in KO-91 cells was nearly twice that in the Ctrl HeLa cells (Fig. 1, F and G), which suggests that loss of WDR91 caused defective recycling of β_2AR back to the plasma membrane. We further examined the distribution of the intracellular cation-independent mannose-6 receptor (CI-MPR). In Ctrl cells, CI-MPR co-localized with both EEA1 and the TGN protein TGN46. The co-localization ratio was higher with TGN46. However, in KO-91 cells, CI-MPR mainly co-localized with EEA1 and its co-localization with TGN46 was strongly decreased (Fig. 1, H and I). This suggests that endosome-to-Golgi recycling of CI-MPR is impaired in the absence of WDR91. Taken together, these findings suggest that WDR91 is required for endosomal recycling of both cell surface and intracellular receptors.

Loss of WDR91 leads to endosomal trapping of SNX-retromer

SNX-BAR-retromer and SNX27-retromer are responsible for recycling of intracellular and cell surface receptors, respectively (Arighi et al., 2004; Bonifacino and Rojas, 2006; Lauffer et al., 2010; Seaman, 2004; Temkin et al., 2011). We thus investigated whether loss of WDR91 affects individual SNX-retromer components. In Ctrl cells, endogenous SNX27 partially co-localized with the early endosomal protein EEA1 and the late endosomal protein Rab7 (Fig. 2, A and B). In KO-91 cells, the co-localization of SNX27 with both EEA1 and Rab7 on the enlarged endosomes was markedly increased (Fig. 2, A and B). Similarly, VPS35 and SNX6 had significantly increased co-localization with EEA1 and Rab7 on the enlarged endosomes in KO-91 cells (Fig. 2, C–F). Because loss of WDR91 causes defective early-to-late endosome conversion and consequently accumulation of enlarged intermediate endosomes, which are positive for both EEA1 and Rab7 (Liu et al., 2016; Liu et al., 2017), these findings suggest that loss of WDR91 resulted in trapping of SNX-retromer complexes on

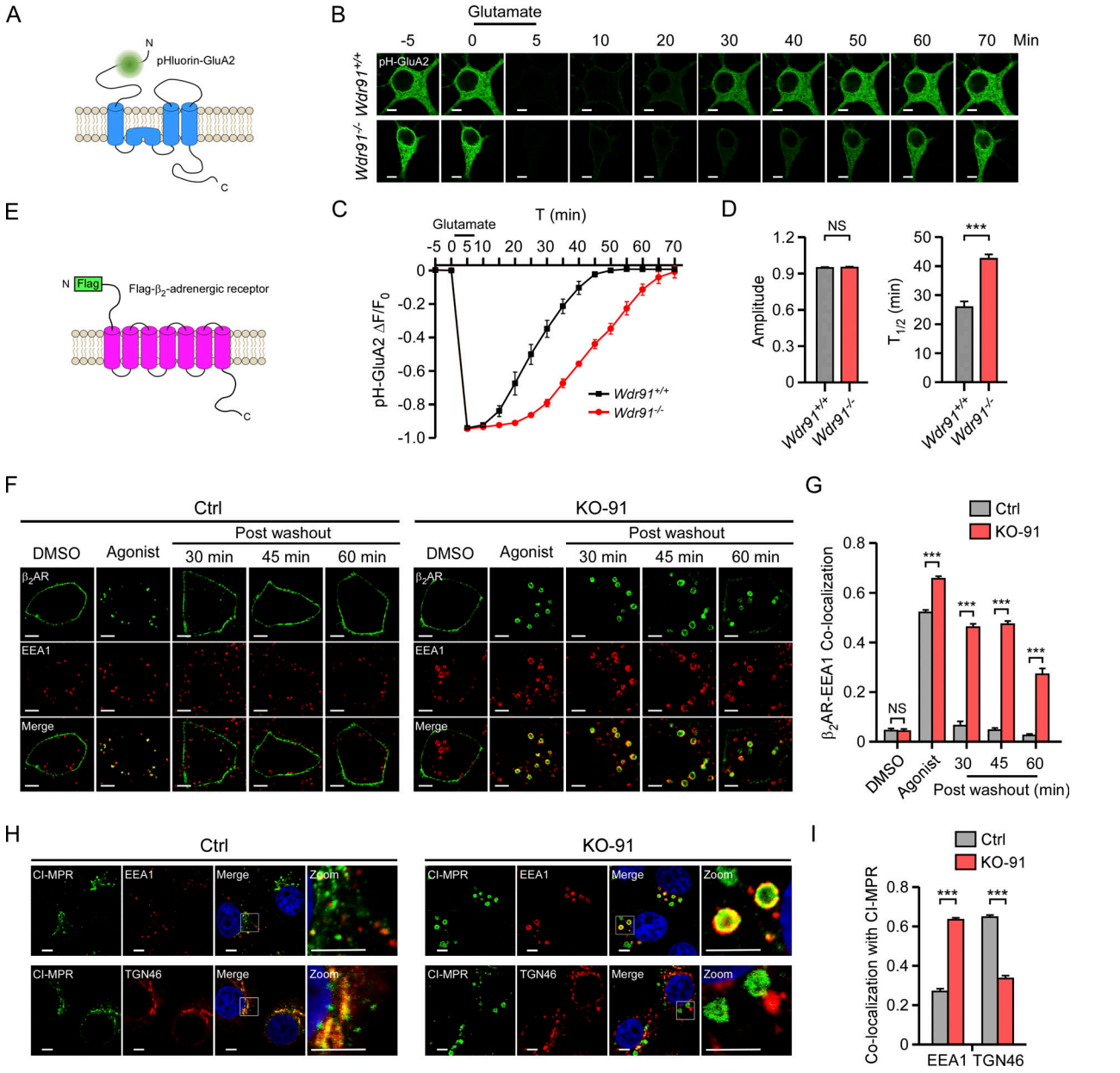

Figure 1. **Loss of WDR91 causes retromer-mediated trafficking defects. (A)** Schematic representation of pH-GluA2. **(B)** Time-course recording of pH-GluA2 in mouse primary hippocampal neurons. Neurons were isolated from *Wdr91*$^{+/+}$ or *Wdr91*$^{-/-}$ mice, transfected with pH-GluA2–expressing vector, and subjected to glutamate perfusion for 5 min. Glutamate was removed at the time point 5 min. Neurons were continuously imaged for pH-GluA2 signals. Bars, 5 µm. **(C)** Time-course tracing of pH-GluA2 fluorescence change in neurons shown in B. *n* = 9 neurons (*Wdr91*$^{+/+}$); *n* = 7 neurons (*Wdr91*$^{-/-}$). **(D)** Left: Maximum amplitudes of pH-GluA2 fluorescence intensity change induced by glutamate. Right: Average half-time ($T_{1/2}$) for recycling after glutamate washout. *n* = 9 neurons (*Wdr91*$^{+/+}$); *n* = 7 neurons (*Wdr91*$^{-/-}$). Statistical analyses were performed with the Mann–Whitney *U*-test. **(E)** Schematic representation of Flag-β_2AR. **(F)** Representative images from a visual trafficking assay of Ctrl and KO-91 HeLa cells expressing Flag-β_2AR. Cells were fixed under the indicated conditions including no treatment (DMSO), isoproterenol perfusion for 30 min (Agonist), and isoproterenol perfusion for 30 min followed by washout and further incubation for the indicated time (Post washout). Bars, 5 µm. **(G)** Quantification of β_2AR-EEA1 co-localization for the indicated treatments as shown in F. The y-axis shows the value of Pearson's correlation coefficient. *n* = 56 cells (Ctrl, DMSO); *n* = 64 cells (KO-91, DMSO); *n* = 61 cells (Ctrl, Agonist); *n* = 99 cells (KO-91, Agonist); *n* = 47 cells (Ctrl, Post washout 30 min); *n* = 42 cells (KO-91, Post washout 30 min); *n* = 45 cells (Ctrl, Post washout 45 min); *n* = 45 cells (KO-91, Post washout 45 min); *n* = 49 cells (Ctrl, Post washout 60 min); *n* = 43 cells (KO-91, Post washout 60 min). Statistical comparisons are between Ctrl and KO-91 cells. Statistical analyses were performed with the two-tailed unpaired *t* test. **(H)** Co-immunostaining of endogenous CI-MPR with EEA1 or TGN46 in Ctrl and KO-91 HeLa cells. Zoom images show magnified frames in the merged images. Bars, 5 µm. **(I)** Quantification of the co-localization of CI-MPR with endosomal or TGN markers as shown in H. The y-axis shows the value of Pearson's correlation coefficient. *n* = 53 cells (Ctrl, CI-MPR-EEA1); *n* = 65 cells (KO-91, CI-MPR-EEA1); *n* = 54 cells (Ctrl, CI-MPR-TGN46); *n* = 46 cells (KO-91, CI-MPR-TGN46). Statistical comparisons are between Ctrl and KO-91 cells. Statistical analyses were performed with the two-tailed unpaired *t* test. For all quantifications, error bars represent SEM. Data are from three independent experiments. ***, P < 0.001. NS, P > 0.05.

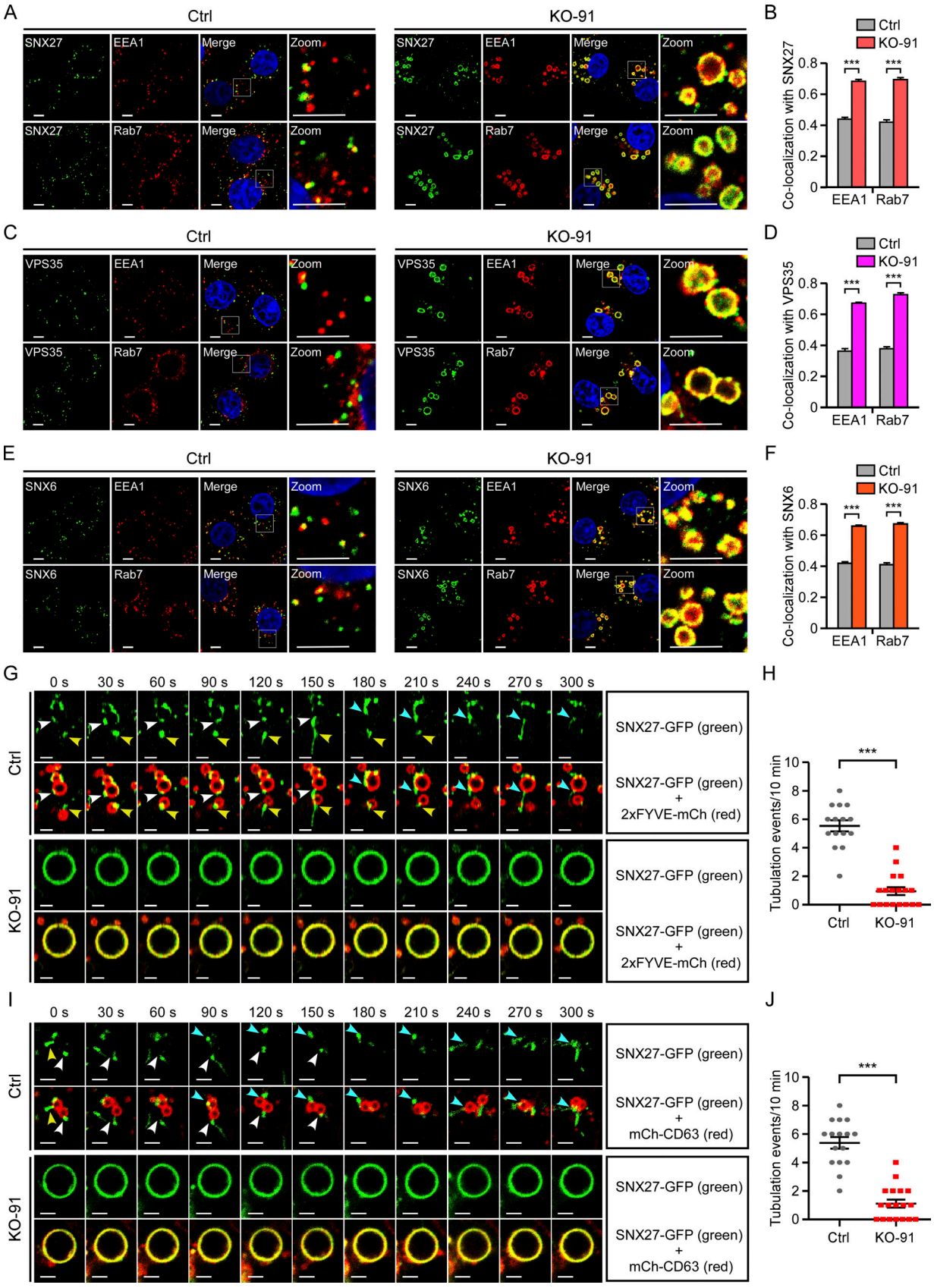

Figure 2. **WDR91 deficiency causes endosomal trapping of SNX-retromer components. (A)** Co-immunostaining of endogenous SNX27 with EEA1 or Rab7 in Ctrl and KO-91 cells. Zoom images show magnified frames in the merged images. Bars, 5 µm. **(B)** Quantification of the co-localization of endogenous SNX27 with endosomal markers as shown in A. *n* = 64 cells (Ctrl, SNX27-EEA1); *n* = 42 cells (KO-91, SNX27-EEA1); *n* = 46 cells (Ctrl, SNX27-Rab7); *n* = 41 cells (KO-91,

SNX27-Rab7). Statistical analyses were performed with the two-tailed unpaired *t* test. **(C)** Co-immunostaining of endogenous VPS35 with EEA1 or Rab7 in Ctrl and KO-91 cells. Zoom images show magnified frames in the merged images. Bars, 5 µm. **(D)** Quantification of the co-localization of endogenous VPS35 with endosomal markers as shown in C. *n* = 40 cells (Ctrl, VPS35-EEA1); *n* = 45 cells (KO-91, VPS35-EEA1); *n* = 45 cells (Ctrl, VPS35-Rab7); *n* = 42 cells (KO-91, VPS35-Rab7). Statistical analyses were performed with the two-tailed unpaired *t* test. **(E)** Co-immunostaining of endogenous SNX6 with EEA1 or Rab7 in Ctrl and KO-91 cells. Zoom images show magnified frames in the merged images. Bars, 5 µm. **(F)** Quantification of the co-localization of endogenous SNX6 with endosomal markers as shown in E. *n* = 54 cells (Ctrl, SNX6-EEA1); *n* = 48 cells (KO-91, SNX6-EEA1); *n* = 45 cells (Ctrl, SNX6-Rab7); *n* = 42 cells (KO-91, SNX6-Rab7). Statistical analyses were performed with the two-tailed unpaired *t* test. **(G)** Time-lapse chasing of SNX27-GFP tubulation events (indicated by arrowheads in different colors) from 2×FYVE-mCh–labeled endosomes in Ctrl and KO-91 cells. For each group, the top row shows SNX27-GFP images and the bottom row shows the merged images of SNX27-GFP and 2×FYVE-mCh. Bars, 2 µm. **(H)** Quantification of SNX27 tubulation events on 2×FYVE-mCh–positive endosomes per cell in 10 min. *n* = 15 cells (Ctrl); *n* = 18 cells (KO-91). Statistical analyses were performed with the Mann–Whitney *U*-test. **(I)** Time-lapse chasing of SNX27-GFP tubulation (indicated by arrowheads in different colors) from mCh-CD63–labeled endosomes in Ctrl and KO-91 cells. For each group, the top row shows SNX27-GFP images and the bottom row shows the merged images of SNX27-GFP and mCh-CD63. Bars, 2 µm. **(J)** Quantification of SNX27 tubulation events on mCh-CD63–positive endosomes per cell 10 min. *n* = 16 cells (Ctrl); *n* = 18 cells (KO-91). Statistical analyses were performed with the Mann–Whitney *U*-test. For all quantifications, error bars represent SEM. Co-localization was quantified according to Pearson's correlation coefficient. Data are from three independent experiments. Statistical comparisons are between Ctrl and KO-91 cells. ***, P < 0.001.

the enlarged intermediate endosomes. To corroborate this point, we performed live-cell imaging to monitor the dynamics of endosomal SNX27. In Ctrl cells, GFP-tagged SNX27 (SNX27-GFP) was enriched in certain subdomains of endosomes labeled with mCherry-tagged 2×FYVE (2×FYVE-mCh), a PtdIns3P marker, or mCherry-CD63 (mCh-CD63), a late endosome membrane protein. SNX27-GFP tubules were further generated and released from these subdomains on either 2×FYVE-mCh– or mCh-CD63–labeled endosomes, which suggests that SNX27-retromer was released from the endosomes (Fig. 2, G–J; and Videos 1 and 2). In KO-91 cells, however, SNX27-GFP was evenly distributed on the enlarged endosomes labeled by either 2×FYVE-mCh or mCh-CD63, and very few SNX27-GFP tubules formed throughout the observation (Fig. 2, G–J; and Videos 1 and 2). Taken together, these findings suggest that WDR91 plays an essential role in SNX-retromer–mediated endosomal recycling.

PtdIns3P contributes differently to endosomal trapping of retromer components in the absence of WDR91

SNXs normally contain a PX domain that binds PtdIns3P (Carlton et al., 2005; Cozier et al., 2002; Lunn et al., 2007; Xu et al., 2001; Zhong et al., 2002), and loss of WDR91 causes elevation of endosomal PtdIns3P (Liu et al., 2016; Liu et al., 2017). Therefore, we investigated whether WDR91-deficiency-induced endosomal trapping of SNXs-retromer depends on PtdIns3P. To do this, we treated cells with VPS34-IN1, a specific inhibitor of the VPS34 kinase. In both Ctrl and KO-91 cells, the co-localization of endogenous SNX27 with EEA1 was significantly decreased by VPS34-IN1 (Fig. 3, A and B). However, VPS34-IN1 did not change the co-localization of SNX27 with Rab7 in KO-91 cells (Fig. 3, C and D). VPS34-IN1 similarly abolished the co-localization of VPS35 with EEA1 but did not change its co-localization with Rab7 on the enlarged endosomes in KO-91 cells (Fig. 3, E–H). Using the PtdIns3P marker 2×FYVE-mCh and the late endosome marker mCh-CD63, we found that both SNX27-GFP and VPS35-GFP clustered at certain subdomains of 2×FYVE-mCh–positive early endosomes or mCh-CD63–labeled late endosomes in Ctrl cells. VPS34-IN1 led to disappearance of endosomal 2×FYVE-mCh, while SNX27-GFP and VPS35-GFP remained clustered at the subdomains of mCh-CD63–labeled late endosomes (Fig. S1, A, C, E and G). On the enlarged intermediate endosomes in KO-91 cells, VPS34-IN1 led to disappearance of endosomal PtdIns3P (2×FYVE-mCh) but did not change the even distribution of SNX27-GFP and VPS35-GFP on mCh-CD63–labeled endosomes (Fig. S1, B, D, F and H). Together these results suggest that endosomal trapping of SNX27-retromer did not result from the elevated PtdIns3P levels induced by WDR91 deficiency.

Within the CSC, VPS35 self-assembles into dimer to promote the formation of arch-like structures (Kendall et al., 2020; Kovtun et al., 2018; Leneva et al., 2021). We asked whether the ability to self-assemble is important for VPS35 clustering. We generated a GFP-fused VPS35 mutant carrying E615A/D616A/E617A/K659E/K662E/K663E (AAA3KE) mutations. The VPS35(AAA3KE) mutant was reported to be devoid of self-assembly capacity (Kendall et al., 2020). We then compared the clustering of GFP-VPS35 and GFP-VPS35(AAA3KE) on 2×FYVE-mCh– or mCh-CD63–labeled endosomes. GFP-VPS35 was clustered at endosomal subdomains on 2×FYVE-mCh– or mCh-CD63–labeled endosomes in Ctrl cells and evenly distributed on endosomes in KO-91 cells. In contrast, GFP-VPS35(AAA3KE) lost the endosomal localization and displayed an even distribution in the cytoplasm in both Ctrl and KO-91 cells (Fig. S1, I–L). These results suggest that VPS35 self-assembly is important for its endosomal localization.

We also examined the effect of VPS34 inhibition on endosomal association of SNX6, SNX2, and SNX3. Similar to SNX27, SNX6, SNX2, and SNX3 were distributed evenly on the enlarged endosomes in KO-91 cells and had a higher co-localization with EEA1 and Rab7 than in Ctrl cells (Fig. S2, A–L). However, VPS34-IN1 treatment abolished their co-localization with EEA1 and Rab7 (Fig. S2, A–L). Thus, in agreement with previous reports (Carlton et al., 2005; Cozier et al., 2002; Xu et al., 2001; Zhong et al., 2002), these findings suggest that SNX-BAR proteins and SNX3 function in a PtdIns3P-dependent manner in retromer-mediated recycling.

Interaction with Rab7 is required for WDR91 to regulate retromer functions

WDR91 is recruited to endosomes by interacting with GTP-bound Rab7 (Liu et al., 2017). To determine whether the interaction with Rab7 is required for WDR91 to regulate retromer function, we examined the rescuing effect of wild-type and Rab7-binding-deficient WDR91 on endosomal trapping of retromer

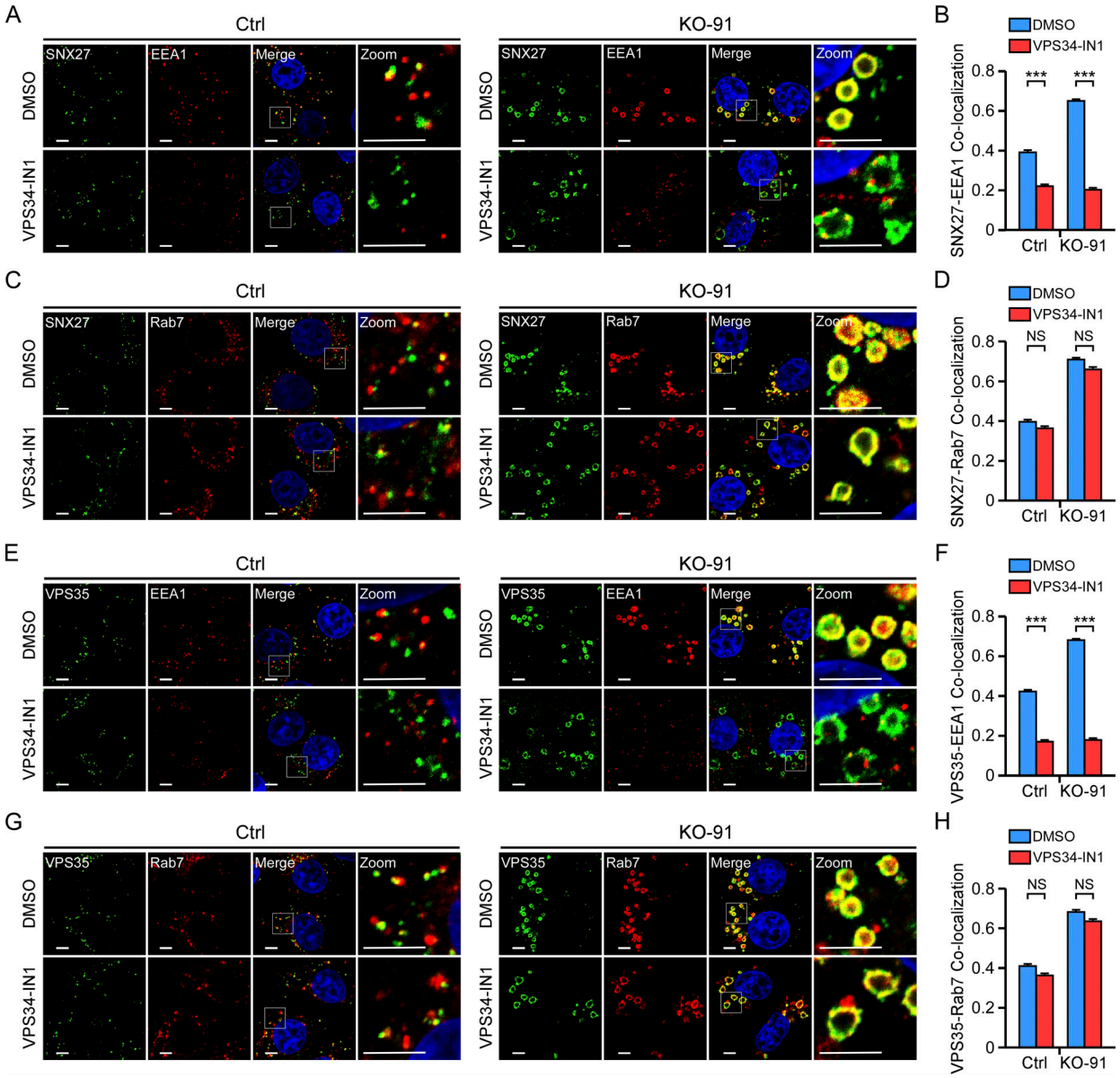

Figure 3. **PtdIns3P contributes differently to endosomal trapping of SNX-retromer components in the absence of WDR91. (A)** Co-immunostaining of endogenous SNX27 with EEA1 in Ctrl and KO-91 cells treated without or with VPS34-IN1 (2 µM) for 3 h. Zoom images show magnified frames in the merged images. Bars, 5 µm. **(B)** Quantification of SNX27-EEA1 co-localization as shown in A. *n* = 64 cells (Ctrl, DMSO); *n* = 56 cells (Ctrl, VPS34-IN1); *n* = 48 cells (KO-91, DMSO); *n* = 56 cells (KO-91, VPS34-IN1). **(C)** Co-immunostaining of endogenous SNX27 with Rab7 in Ctrl and KO-91 cells treated without or with VPS34-IN1 (2 µM) for 3 h. Zoom images show magnified frames in the merged images. Bars, 5 µm. **(D)** Quantification of SNX27-Rab7 co-localization as shown in C. *n* = 57 cells (Ctrl, DMSO); *n* = 57 cells (Ctrl, VPS34-IN1); *n* = 58 cells (KO-91, DMSO); *n* = 72 cells (KO-91, VPS34-IN1). **(E)** Co-immunostaining of endogenous VPS35 with EEA1 in Ctrl and KO-91 cells treated without or with VPS34-IN1 (2 µM) for 3 h. Zoom images show magnified frames in the merged images. Bars, 5 µm. **(F)** Quantification of VPS35-EEA1 co-localization as shown in E. *n* = 60 cells (Ctrl, DMSO); *n* = 83 cells (Ctrl, VPS34-IN1); *n* = 45 cells (KO-91, DMSO); *n* = 55 cells (KO-91, VPS34-IN1). **(G)** Co-immunostaining of endogenous VPS35 with Rab7 in Ctrl and KO-91 cells treated without or with VPS34-IN1 (2 µM) for 3 h. Zoom images show magnified frames in the merged images. Bars, 5 µm. **(H)** Quantification of VPS35-Rab7 co-localization as shown in G. *n* = 42 cells (Ctrl, DMSO); *n* = 52 cells (Ctrl, VPS34-IN1); *n* = 44 cells (KO-91, DMSO); *n* = 48 cells (KO-91, VPS34-IN1). For all quantifications, error bars represent SEM. The y-axis shows the value of Pearson's correlation coefficient. Data are from three independent experiments. Statistical comparisons are between DMSO and VPS34-IN1 treatments. Statistical analyses were performed with the Kruskal–Wallis test. ***, P < 0.001. NS, P > 0.05.

components. We used two WDR91 mutants which are unable to interact with Rab7: one carries the F570A/N571A/H572A mutations (Flag-WDR91[3A]) and the other has a deletion of aa159-163 (Flag-WDR91[Δ5]; Liu et al., 2017). In KO-91 cells, expression of Flag-WDR91 strongly reduced the trapping of SNX27 on mCh-CD63–positive endosomes and enabled SNX27 to localize to endosomal subdomains (Fig. 4, A and B). In contrast, expression of Flag-WDR91(3A) or Flag-WDR91(Δ5) had no rescuing effect on endosomal trapping of SNX27 (Fig. 4, A and B). Similarly, wild-type WDR91, but not WDR91(3A) or WDR91(Δ5), abolished the even distribution of VPS35 and instead led to its localization to certain subdomains on mCh-CD63–labeled

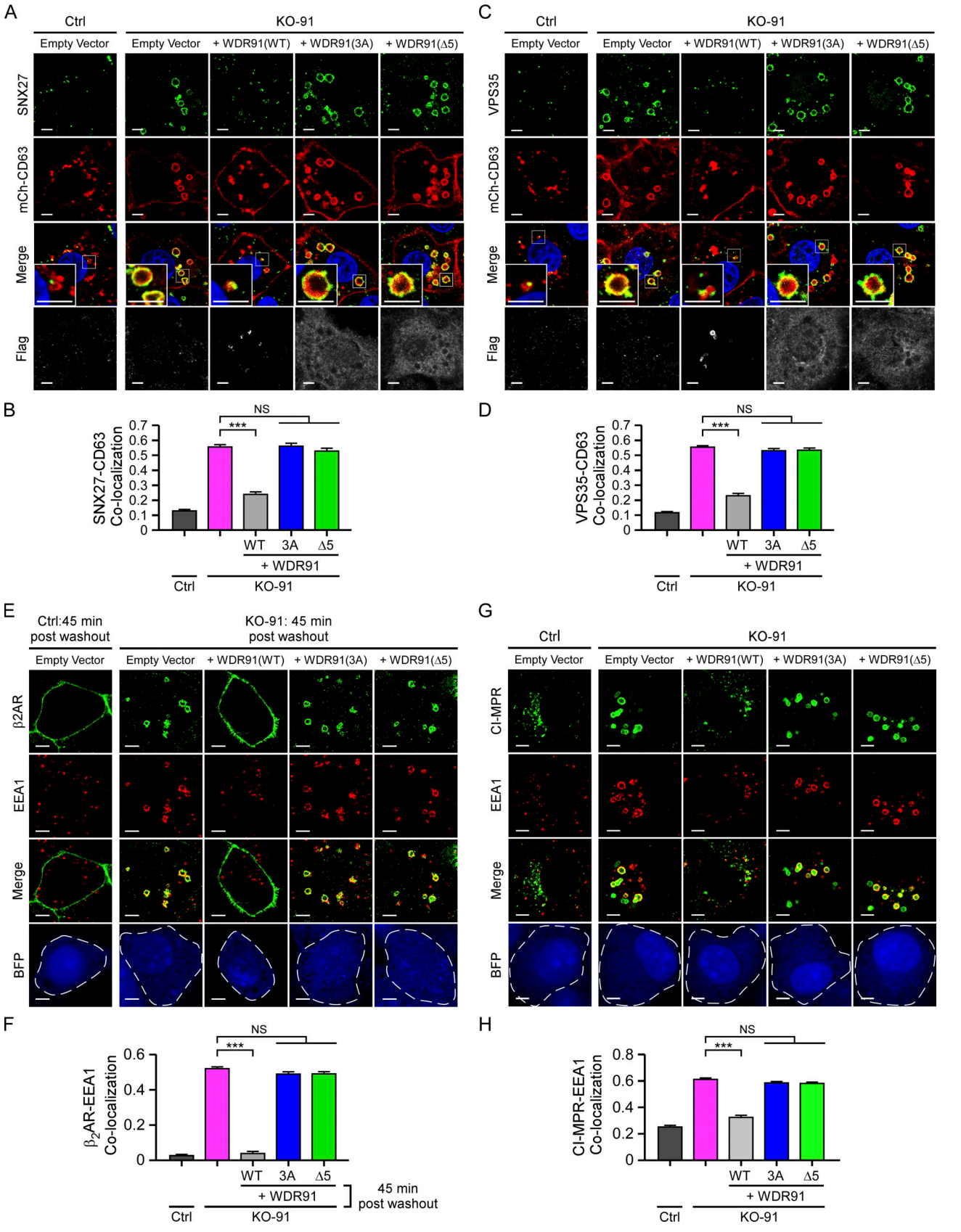

Figure 4. **Interaction with Rab7 is required for WDR91 to regulate SNX-retromer function. (A)** Rescue of endosomal trapping of SNX27 by Flag-WDR91, Flag-WDR91(3A), and Flag-WDR91(Δ5) in KO-91 cells. Ctrl and KO-91 cells were co-transfected with vectors expressing the indicated Flag-WDR91 proteins and mCh-CD63. 24 h later, the cells were fixed and stained with SNX27 and Flag antibodies. In the merged images, the boxed regions are magnified at the bottom

left. Bars, 5 µm. **(B)** Quantification of the co-localization of SNX27 with mCh-CD63 as shown in A. *n* = 40 cells (Ctrl); *n* = 42 cells (KO-91, empty); *n* = 32 cells (KO-91, + WDR91[WT]); *n* = 35 cells (KO-91, + WDR91[3A]); *n* = 36 cells (KO-91, + WDR91[Δ5]). **(C)** Rescue of endosomal trapping of VPS35 by Flag-WDR91, Flag-WDR91(3A), and Flag-WDR91(Δ5) in KO-91 cells. Ctrl and KO-91 cells were transfected with vectors expressing the indicated Flag-WDR91 proteins and mCh-CD63. 24 h later, the cells were fixed and stained with VPS35 and Flag antibodies. In the merged images, the boxed regions are magnified at the bottom left. Bars, 5 µm. **(D)** Quantification of the co-localization of VPS35 with mCh-CD63 as shown in C. *n* = 37 cells (Ctrl); *n* = 45 cells (KO-91, empty); *n* = 31 cells (KO-91, + WDR91[WT]); *n* = 36 cells (KO-91, + WDR91[3A]); *n* = 38 cells (KO-91, + WDR91[Δ5]). **(E)** Rescue of defective β_2ARs recycling by Myc-WDR91, Myc-WDR91(3A), and Myc-WDR91(Δ5) in KO-91 cells. Ctrl and KO-91 cells were transfected with vectors expressing Flag-β_2AR, Myc-WDR91 proteins and BFP (the marker for transfected cells). 24 h later, the cells were subjected to isoproterenol treatment and washout. 45 min after washout, the cells were fixed for immunostaining. Bars, 5 µm. **(F)** Quantification of the co-localization of Flag-β_2ARs with EEA1 as shown in E. *n* = 44 cells (Ctrl); *n* = 42 cells (KO-91, empty); *n* = 47 cells (KO-91, + WDR91[WT]); *n* = 47 cells (KO-91, + WDR91[3A]); *n* = 46 cells (KO-91, + WDR91[Δ5]). **(G)** Rescue of defective CI-MPR trafficking by Flag-WDR91, Flag-WDR91(3A), and Flag-WDR91(Δ5) in KO-91 cells. Ctrl and KO-91 cells were transfected with vectors expressing the indicated Flag-WDR91 proteins and BFP. 24 h later, the cells were fixed and stained with CI-MPR and EEA1 antibodies. Bars, 5 µm. **(H)** Quantification of the co-localization of CI-MPR with EEA1 as shown in G. *n* = 46 cells (Ctrl); *n* = 52 cells (KO-91, empty); *n* = 50 cells (KO-91, + WDR91[WT]); *n* = 48 cells (KO-91, + WDR91[3A]); *n* = 52 cells (KO-91, + WDR91[Δ5]). For all quantifications, error bars represent SEM. The y-axis shows the value of Pearson's correlation coefficient. Data are from three independent experiments. Statistical analyses were performed with one-way ANOVA with Tukey's post hoc test. ***, P < 0.001. NS, P > 0.05.

endosomes in KO-91 cells (Fig. 4, C and D). Consistent with this, wild-type WDR91, but not the WDR91(3A) and WDR91(Δ5) mutants, successfully rescued the defective endosome-plasma membrane recycling of β_2AR in KO-91 cells (Fig. 4, E and F). The glutamate-induced pH-GluA2 trafficking defects in *Wdr91*$^{-/-}$ neurons were rescued by wild-type WDR91 but not the Rab7-binding-deficient mutants (Fig. S3, A–C). In addition, wild-type WDR91, but not the Rab7-binding-deficient mutants, inhibited the strong increase of endosomal CI-MPR (Fig. 4, G and H). Collectively, these findings suggest that endosomal recruitment of WDR91 by Rab7 is essential for appropriate endosomal localization and function of SNX-retromer.

WDR91 promotes the interaction of Rab7 with retromer components

We next investigated whether WDR91 interacts with individual SNX-retromer components. In co-immunoprecipitation (co-IP) assays, Flag-WDR91 co-precipitated with GFP-SNX27 (Fig. 5 A). SNX27 contains a PDZ domain, a PX domain and a FERM domain (Fig. 5 B). GFP-SNX27(PX), which contains the PX domain (aa159–273), co-precipitated with the full-length WDR91 (Fig. 5, B and D). Other SNX27 domains did not co-precipitate with WDR91 (Fig. 5, B, C and E). We similarly investigated the requirement for WDR91 domains to interact with SNX27 (Fig. 5 F). Flag-WDR91(392-747), which contains the C-terminal WD40-repeats, co-precipitated with GFP-SNX27(PX) (Fig. 5 G). Thus, the PX domain of SNX27 and the WD40-repeats of WDR91 mediate the interaction of these two proteins. In vitro, GST-fused SNX27 pulled down His_6-fused WDR91 (WDR91-His_6; Fig. 5 H), and GST-fused SNX27(PX) pulled down WDR91-His_6 and His_6-WDR91(392-747) (Fig. S4 A and Fig. 5 I). These results suggest that WDR91 and SNX27 directly interact with one another. In co-IP assays, GFP-SNX27(PX) co-precipitated Flag-WDR91 in the presence of VPS34-IN1 (Fig. S4 B). Moreover, GFP-SNX27(PX) containing RYKR/AAAA mutations in the PX domain (GFP-SNX27[PX-RYKR/4A]), which abolish the PtdIn3P-binding capacity (Chandra et al., 2019), also co-precipitated with Flag-WDR91 (Fig. S4 B). Collectively, these findings suggest that the interaction of SNX27 with WDR91 does not depend on PtdIns3P. In co-IP assays, WDR91 also co-precipitated with individual SNX1, 2, 5, 6, and 3 proteins, and their PX domains (Fig. S4, C–Q). GST-fused SNX1, 2, 5, 6, and 3, as well as the GST-fused PX domain of these SNXs, interacted with WDR91-His_6 in GST pull-down assays (Fig. S4, R and S). Thus, WDR91 directly interacts with SNX-BAR proteins and SNX3 through the PX domain, and these interactions do not require the presence of PtdIns3P.

Because SNX27 and VPS35 localize to Rab7-positive endosomes, we next investigated whether SNX27 and VPS35 interact with Rab7. In co-IP assays, Myc-SNX27 failed to co-precipitate with GFP-Rab7(WT), or the constitutively active GFP-Rab7(Q67L), or the inactive GFP-Rab7(T22N) (Fig. 5 J). This suggests that no direct interaction occurs between SNX27 and Rab7. We then tested whether WDR91 bridges the interaction of Rab7 with SNX27. In co-IP assays, Myc-SNX27 co-precipitated with GFP-Rab7(Q67L) in the presence of Flag-WDR91 (Fig. 5 K), suggesting that WDR91 forms a complex with the active Rab7 and SNX27. The Rab7-binding-deficient WDR91(3A) and WDR91(Δ5) mutants, which do not localize to endosomes (Liu et al., 2017), were able to interact with GFP-SNX27(PX) (Fig. 5 L); however, they failed to form a tripartite complex with Rab7 and SNX27 in co-IP assays (Fig. 5 M). In addition, no obvious interaction was detected between GFP-Rab7(T22N) and Myc-SNX27 even in the presence of wild-type WDR91 (Fig. 5 M). Taken together, these findings suggest that WDR91 promotes the interaction of active Rab7 with SNX27 on endosomes.

GFP-VPS35 also co-precipitated with Flag-WDR91 in co-IP assays (Fig. 5 N) and GST-VPS35 interacted with WDR91-His_6 in vitro (Fig. 5 O). Nevertheless, Myc-VPS35 was not obviously co-precipitated with GFP-Rab7(Q67L) (Fig. 5 P), consistent with previous reports (Rojas et al., 2008). In the presence of Flag-WDR91, however, Myc-VPS35 co-precipitated with GFP-Rab7(Q67L) (Fig. 5 P). To rule out the possibility that this interaction involves VPS26, we tested the co-IP of WDR91 with GFP-VPS35 containing R107A and L108P mutations in the conserved PRLYL motif (GFP-VPS35[RL/AP]). Previous studies showed that these two mutations abolished the interaction of VPS35 with VPS26 (Gokool et al., 2007; Norwood et al., 2011). In agreement with the previous reports, we found that GFP-VPS35(RL/AP) failed to associate with Myc-VPS26; however, it was co-precipitated with Flag-WDR91 (Fig. S4, T and U). Taken together, these results suggest that WDR91 likely interacts with VPS35 directly to promote the interaction of VPS35 with active Rab7, and this event probably does not require VPS26. Supporting this point, ectopically expressed GFP-Rab7(Q67L) pulled

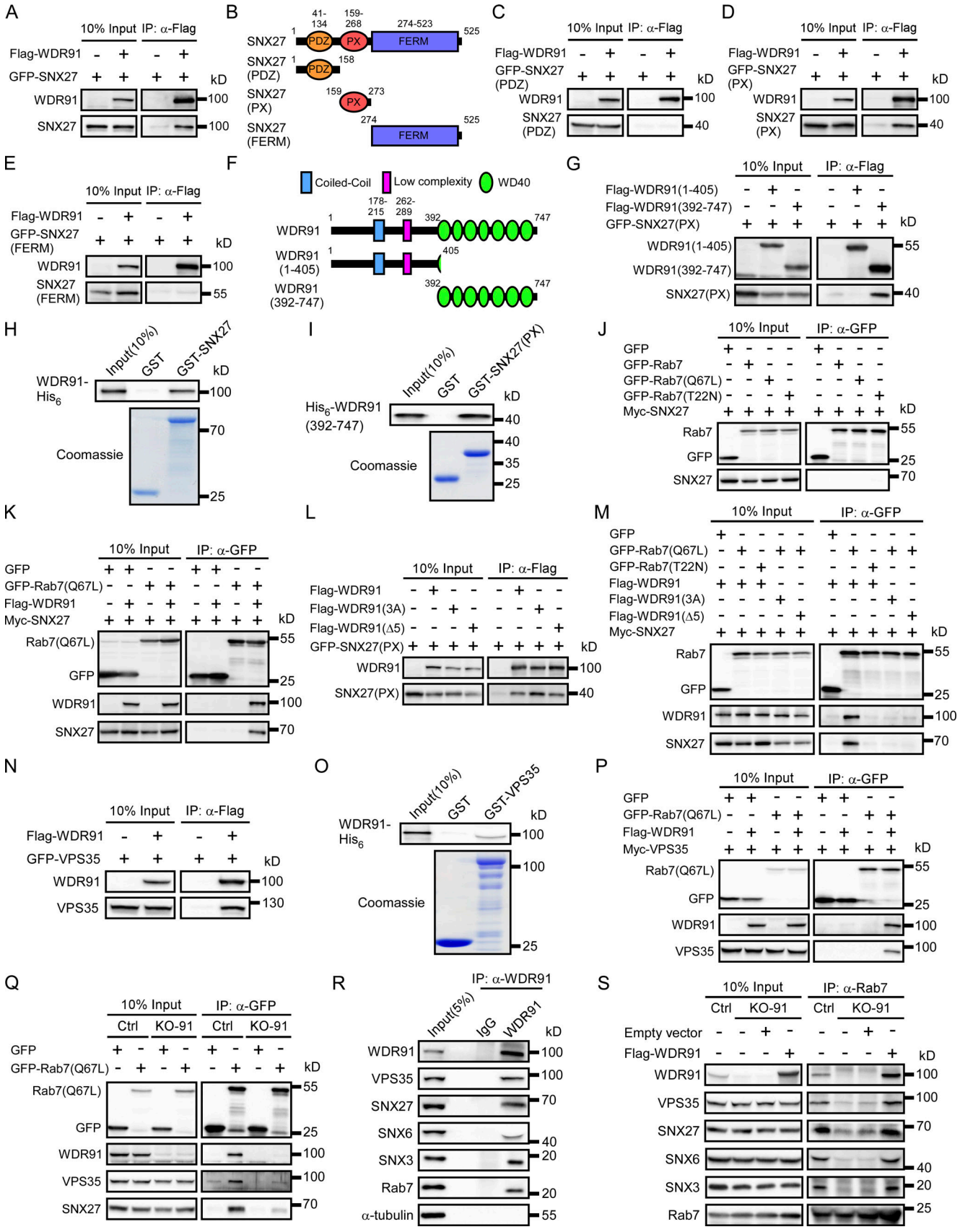

Figure 5. **WDR91 promotes Rab7 interaction with SNX-retromer components. (A)** Co-IP of Flag-WDR91 with GFP-SNX27. IP was performed with anti-Flag antibody resin and the precipitated proteins were detected with Flag and GFP antibodies. **(B)** Schematic depiction of SNX27 truncations. **(C–E)** Co-IP of

Flag-WDR91 with GFP-tagged PDZ (C), PX (D), and FERM (E) of SNX27. IPs were performed with anti-Flag antibody resin and detected with Flag and GFP antibodies. **(F)** Schematic depiction of WDR91 truncations. **(G)** Co-IP of Flag-tagged WDR91(1-405) and WDR91(392-747) with GFP-SNX27(PX). IPs were performed with anti-Flag antibody resin and detected with Flag and GFP antibodies. **(H)** GST and GST-SNX27 immobilized on glutathione-Sepharose beads were incubated with WDR91-His_6. The precipitates were immunoblotted with His_6 antibody. GST-fusion proteins were stained with Coomassie blue. **(I)** GST and GST-SNX27(PX) immobilized on glutathione-Sepharose beads were incubated with His_6-WDR91(392-747). The precipitates were immunoblotted with His_6 antibody. GST-fusion proteins were stained with Coomassie blue. **(J)** Co-IP of GFP-tagged Rab7(WT), Rab7(Q67L), and Rab7(T22N) with Myc-SNX27. IPs were performed with GFP-trap beads, and precipitated proteins were detected with Myc and GFP antibodies. **(K)** Co-IP of GFP-Rab7(Q67L) with Myc-SNX27 without or with Flag-WDR91. IPs were performed with GFP-trap beads and immunoblotted using Flag, Myc, and GFP antibodies. **(L)** Co-IP of Flag-WDR91(WT), Flag-WDR91(3A), and Flag-WDR91(Δ5) with GFP- SNX27(PX). IPs were performed with anti-Flag antibody resin and immunoblotted using Flag and GFP antibodies. **(M)** Co-IP of Myc-SNX27 with GFP-Rab7(Q67L) or GFP-Rab7(T22N) in the presence of Flag-WDR91(WT), Flag-WDR91(3A), or Flag-WDR91(Δ5). IPs were performed with GFP-trap beads and immunoblotted using Flag, Myc and GFP antibodies. **(N)** Co-IP of Flag-WDR91 with GFP-VPS35. IPs were performed with anti-Flag antibody resin and immunoblotted using Flag and GFP antibodies. **(O)** GST and GST-VPS35 immobilized on glutathione-Sepharose beads were incubated with WDR91-His_6. The precipitates were immunoblotted with His_6 antibody. GST-fusion proteins were stained with Coomassie blue. **(P)** Co-IP of GFP-Rab7(Q67L) with Myc-VPS35 in the presence of Flag-WDR91. IPs were performed with GFP-trap beads and immunoblotted using Flag, Myc, and GFP antibodies. **(Q)** Co-IP of endogenous VPS35, SNX27, and WDR91 with ectopically expressed GFP-Rab7(Q67L) in control and KO-91 HeLa cells. Proteins were precipitated with GFP-trap beads and detected with antibodies against GFP, WDR91, VPS35, and SNX27. **(R)** Co-IP of endogenous VPS35, SNX27, SNX6, SNX3, and Rab7 with WDR91 in control HeLa cells. IPs were performed with WDR91 antibody and precipitated proteins were detected with antibodies against the indicated proteins. **(S)** Co-IP of endogenous WDR91, VPS35, SNX27, SNX6, and SNX3 with Rab7 in Ctrl cells, KO-91 cells, and KO-91 cells transfected with empty or Flag-WDR91–expressing vectors. IPs were performed with Rab7 antibody and precipitated proteins were detected with antibodies against the indicated proteins. Source data are available for this figure: SourceData F5.

down endogenous WDR91, VPS35, and SNX27 in Ctrl HeLa cells, while the association of endogenous VPS35 and SNX27 with GFP-Rab7(Q67L) was greatly reduced in KO-91 cells (Fig. 5 Q).

We finally examined whether the interaction of WDR91 with Rab7 and SNX-retromer components exists at the endogenous level. Using WDR91 antibody for co-IP assays, we found that endogenous Rab7, VPS35, SNX27, SNX6, and SNX3 were co-precipitated with WDR91 in Ctrl cells (Fig. 5 R). Endogenous WDR91, VPS35, SNX27, SNX6, and SNX3 were also co-immunoprecipitated with Rab7 (Fig. 5 S). These data suggest that these endogenous proteins indeed interact in the cell. In KO-91 cells, the co-precipitation of endogenous VPS35, SNX27, SNX6, and SNX3 with Rab7 was strongly decreased. When Flag-WDR91 was introduced into KO-91 cells, these proteins co-precipitated with Rab7 again (Fig. 5 S). These results provide further evidence that WDR91 promotes the interaction of Rab7 with SNX-retromer components.

WDR91 enriches and restricts active Rab7 and SNX-retromer components at the retrieval subdomain

To pinpoint the function of WDR91 interaction with the active Rab7 and SNX-retromer on endosomes, we developed a fluorescent detector that senses the activation status of Rab7. PLEKHM1 is a Rab7 effector that contains two PH domains (PH1 and PH2) and a C1 domain (Fig. 6 A; McEwan et al., 2015a; McEwan et al., 2015b). In co-IP assays, Myc-tagged PH2-C1 of PLEKHM1 (Myc-PH2C1) co-precipitated with GFP-Rab7(WT) and the constitutively active GFP-Rab7(Q67L), but not the inactive GFP-Rab7(T22N) (Fig. 6 B). Consistent with this, mCherry-fused PH2C1 (mCh-PH2C1) co-localized with GFP-Rab7(WT) and GFP-Rab7(Q67L), but not with GFP-Rab7(T22N), on endosomes (Fig. 6 C). Thus, PH2C1 tagged with a fluorescent protein can be used as a specific detector for active Rab7.

Using mCh-PH2C1, we analyzed the endosomal distribution of active Rab7. In Ctrl cells, mCh-PH2C1 was enriched at certain endosomal subdomains. In KO-91 cells, however, mCh-PH2C1 was evenly distributed on endosomes. Reinforced expression of WDR91 restored the enrichment of mCh-PH2C1 at specific endosomal subdomains in KO-91 cells (Fig. 6 D). Of note, the function of restricting active Rab7 on endosomal subdomains is specific to WDR91, because reinforced expression of RILP and FYCO1, two other Rab7 effectors (Cantalupo et al., 2001; Pankiv et al., 2010), failed to induce Rab7 enrichment at endosomal subdomains in KO-91 cells (Fig. 6 D). mCh-PH2C1 enrichment at endosomal subdomains was further confirmed by measuring the fluorescence intensity along the endosome surface (Fig. 6 E). Using the FRAP assay, we found that, following fluorescence photo-bleaching, the recovery of the endosomal subdomain-enriched mCh-PH2C1 signals in Ctrl cells was much slower than that of the evenly distributed endosomal mCh-PH2C1 in KO-91 cells (Fig. 6, F and G). In KO-91 cells, reinforced expression of WDR91 enabled mCh-PH2C1 to enrich at specific endosomal subdomains, and mCh-PH2C1 signals recovered at an even slower rate than in Ctrl cells in FRAP assays (Fig. 6, F and G). Taken together, these results suggest that WDR91 enriches and restricts active Rab7 at specific endosomal subdomains.

We next investigated the effect of WDR91 on endosomal distribution of SNX-retromer components. In Ctrl cells, SNX27-GFP, SNX6-GFP, and VPS35-GFP were enriched and co-localized with the active Rab7 (indicated by mCh-PH2C1) at an endosomal subdomain (Fig. 6 H). In contrast, they were evenly distributed on endosomes in KO-91 cells (Fig. 6 I). When BFP-WDR91 was introduced into KO-91 cells, these factors were re-enriched and co-localized with BFP-WDR91 at endosomal subdomains (Fig. 6 J). These findings suggest that WDR91 is essential and sufficient to cluster active Rab7 and SNX-retromer components to WDR91-specific endosomal subdomains. Using time-lapse imaging, we further found that SNX27-GFP and VPS35-GFP progressively formed tubules at the mCh-WDR91–enriched domains, which were eventually released from endosomes (Fig. 6, K and L; and Videos 3 and 4). Taken together, these findings suggest that WDR91 defines the retrieval subdomain on endosomes, from which Rab7-dependent and SNX-retromer–mediated retrieval and recycling take place.

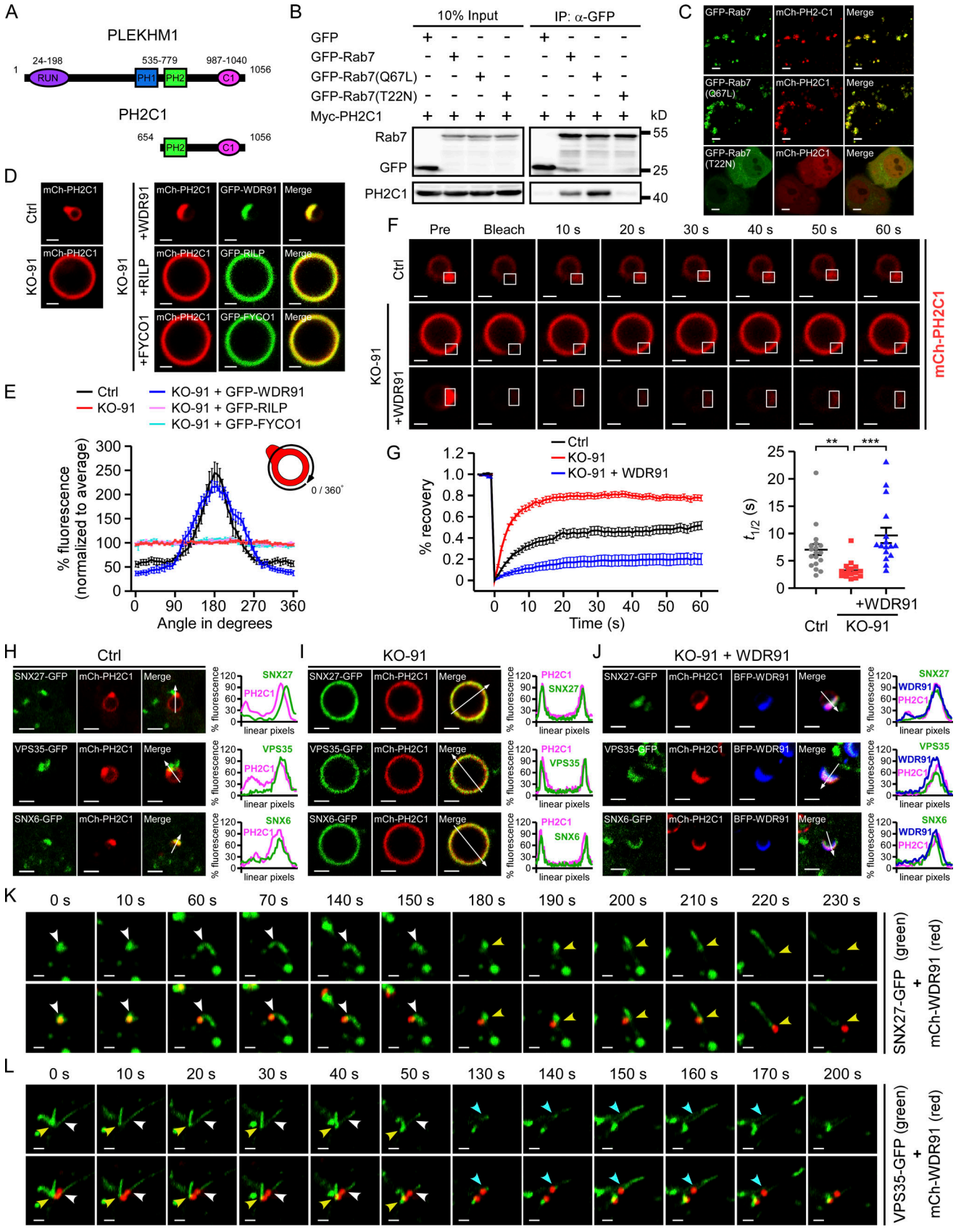

Figure 6. **WDR91 enriches and restricts active Rab7 and SNX-retromer components for formation of the endosomal retrieval subdomain. (A)** Schematic depiction of an active Rab7-detecting sensor derived from the PH2-C1 domain of PLEKHM1. **(B)** Co-IP of GFP-Rab7, GFP-Rab7(Q67L), and Rab7(T22N) with Myc-PH2C1. IPs were performed with GFP-trap beads and immunoblotted using Myc and GFP antibodies. **(C)** Co-localization of mCherry-

PH2C1 (mCh-PH2C1) with GFP-Rab7, GFP-Rab7(Q67L), and GFP-Rab7(T22N) in HeLa cells. Bars, 5 µm. **(D)** Representative images of endosomal mCh-PH2C1 in Ctrl cells, KO-91 cells, and KO-91 cells expressing GFP-WDR91, GFP-RILP, or GFP-FYCO1. Bars, 1 µm. **(E)** Measurement of mCh-PH2C1 fluorescence intensity in a clockwise direction along the endosomal membrane (as indicated in the upper right) as shown in D. n = 12 endosomes (Ctrl); n = 12 endosomes (KO-91); n = 12 endosomes (KO-91 + GFP-WDR91); n = 12 endosomes (KO-91 + GFP-RILP); n = 12 endosomes (KO91 + GFP-FYCO1). The profiles of endosomes were obtained and normalized to achieve the average endosomal mCh-PH2C1 fluorescence intensity (mean ± SEM). **(F)** FRAP analysis of mCh-PH2C1 in Ctrl, KO-91 cells, and KO-91 cells re-expressing WDR91. The frame in each individual image indicates the photo-bleached area. Bars, 1 µm. **(G)** Quantification of fluorescence recovery of mCh-PH2C1 (left), and recovery half-time ($t_{1/2}$; right). n = 18 endosomes (Ctrl); n = 16 endosomes (KO-91); n = 16 endosomes (KO-91 + WDR91). Data represent mean ± SEM. Statistical analyses were performed with the Kruskal–Wallis test. **, P < 0.01; ***, P < 0.001. **(H and I)** Co-localization of SNX27-GFP, VPS35-GFP, SNX6-GFP with mCh-PH2C1 in Ctrl (H) and KO-91(I) HeLa cells. Quantifications of linear pixel fluorescence of GFP-tagged proteins (green) and mCh-PH2C1 (magenta) along the arrows across the endosomes in the merge images are shown on the right. Bars, 2 µm. **(J)** Co-localization of SNX27-GFP, VPS35-GFP, SNX6-GFP with mCh-PH2C1 in KO-91 cells re-expressing BFP-WDR91. Quantifications of linear pixel fluorescence of GFP-tagged proteins (green), mCh-PH2C1 (magenta), and BFP-WDR91 (blue) along the arrows across the endosomes in the merge images are shown on the right. Bars, 2 µm. **(K and L)** Time-lapse chasing of SNX27-GFP–labeled (K) or VPS35-GFP–labeled (L) tubulation events (indicated by arrowheads in different colors) from mCh-WDR91–enriched endosomal domains. Bars, 1 µm. Source data are available for this figure: SourceData F6.

WDR81 acts through WDR91 to regulate endosomal retrieval subdomain formation

WDR81 and WDR91 form a complex which inhibits endosomal PtdIns3P synthesis to facilitate early-to-late endosome conversion (Liu et al., 2016; Rapiteanu et al., 2016). We investigated whether WDR81 is also important for formation of endosomal retrieval subdomains and the recycling of membrane receptors. In both Ctrl and *WDR81* knockout (KO-81) HeLa cells, isoproterenol induced β_2AR internalization to EEA1-positive endosomes. However, the recycling of β_2AR to the plasma membrane following removal of the agonist was strongly inhibited in KO-81 cells (Fig. 7, A and B). The intracellular CI-MPR was also trapped on the enlarged endosomes in KO-81 cells (Fig. 7, C and D). These results suggest that WDR81 is important for recycling of both intracellular and cell surface receptors. Furthermore, the active Rab7, as indicated with mCh-PH2C1, was evenly distributed on the enlarged endosomes in KO-81 cells, suggesting that loss of WDR81 impaired the formation of endosomal retrieval subdomains (Fig. 7, E and F). Reinforced expression of GFP-WDR81 restored the enrichment of mCh-PH2C1 at specific endosomal subdomains. Importantly, reinforced expression of GFP-WDR91 similarly restored the enrichment of mCh-PH2C1 at endosomal subdomains in KO-81 cells (Fig. 7, E and F). In contrast, ectopically expressed GFP-WDR81 exhibited a cytoplasmic distribution in KO-91 cells and did not co-localize with mCh-PH2C1 on endosomes (Fig. 7, G and H). When BFP-WDR91 was co-expressed with GFP-WDR81, both mCh-PH2C1 and GFP-WDR81 were clustered at WDR91-specific endosomal subdomains (Fig. 7, G and H). Together these findings suggest that WDR81 is recruited by WDR91 to endosomal retrieval subdomains containing active Rab7. Consistent with these findings, WDR91, like WDR81, successfully rescued the defective endosome-to-plasma membrane recycling of β_2AR (Fig. 7, A and B) and the endosomal trapping of CI-MPR (Fig. 7, C and D) in KO-81 cells. Taken together, these findings suggest that WDR81 acts through WDR91 to affect endosomal retrieval subdomain formation and recycling of membrane receptors.

WDR91 facilitates actin organization for formation of retrieval subdomains

Given that the endosomal actin network is required for endosomal cargo retrieval and recycling by retromer (Puthenveedu et al., 2010; Simonetti and Cullen, 2019), we investigated whether WDR91 plays a role in endosomal actin organization. In Ctrl cells, the F-actin foci, visualized by Phalloidin staining, localized in close proximity to Rab7-positive endosomes (Fig. 8 A). In KO-91 cells, however, F-actin evenly surrounded the enlarged Rab7-positive endosomes (Fig. 8 A). These results suggest that loss of WDR91 impaired endosomal actin organization. Because the formation of endosomal actin networks is mediated by the Arp2/3 complex, which is activated by nucleation promoting factors (NPFs) including the WASH complex (Derivery et al., 2009; Gomez and Billadeau, 2009), we examined whether WDR91 deficiency affects endosomal recruitment and distribution of Arp2/3 and/or NPFs. In Ctrl cells, ARPC2 (a subunit of the Arp2/3 complex) and FAM21 (a core subunit of WASH) showed focal localization and partly overlapped with Rab7. In sharp contrast, ARPC2 and FAM21 were distributed evenly around Rab7-positive late endosomes in KO-91 cells (Fig. 8 B). This suggests that WDR91 is important for the distribution of Arp2/3 and NPFs on endosomes, but does not affect their recruitment to endosomes. Interestingly, VPS34-IN1 did not change the distribution pattern of ARPC2 and FAM21 on Rab7-positive endosomes in both Ctrl and KO-91 cells (Fig. S5, A–D), suggesting that the endosomal localization of Arp2/3 and NPFs is independent of PtdIns3P.

We next examined whether WDR91 interacts with Arp2/3 and FAM21. In co-IP assays, GFP-WDR91 co-precipitated with Flag-FAM21 (Fig. 8 C), but not Myc-tagged ARP2 or ARP3 (Fig. S5, E and F). Consistent with this, endogenous FAM21 is associated with immunoprecipitated WDR91 (Fig. 8 D). Together these results suggest that WDR91 and FAM21 interact with one another in the cell. Flag-FAM21 also interacted with GFP-SNX27 and GFP-VPS35 (Fig. S5, G and H), as reported previously (Harbour et al., 2012; Jia et al., 2012; Lee et al., 2016; Steinberg et al., 2013). Given that WDR91 forms a complex with active Rab7, SNX27, and VPS35, these results suggest that WDR91 likely regulates endosomal distribution of FAM21 together with Rab7 and SNX27-retromer. Supporting this hypothesis, GFP-FAM21 localized to an endosomal subdomain enriched with active Rab7 (mCh-PH2C1) in Ctrl cells. In contrast, both FAM21 and active Rab7 were evenly distributed on endosomes in KO-91 cells (Fig. 8 E). Following expression of BFP-WDR91 in KO-91 cells, both GFP-FAM21 and active Rab7 (mCh-PH2C1) were clustered at WDR91-enriched endosomal subdomains (Fig. 8 E). Thus, WDR91 promotes FAM21 enrichment at endosomal retrieval

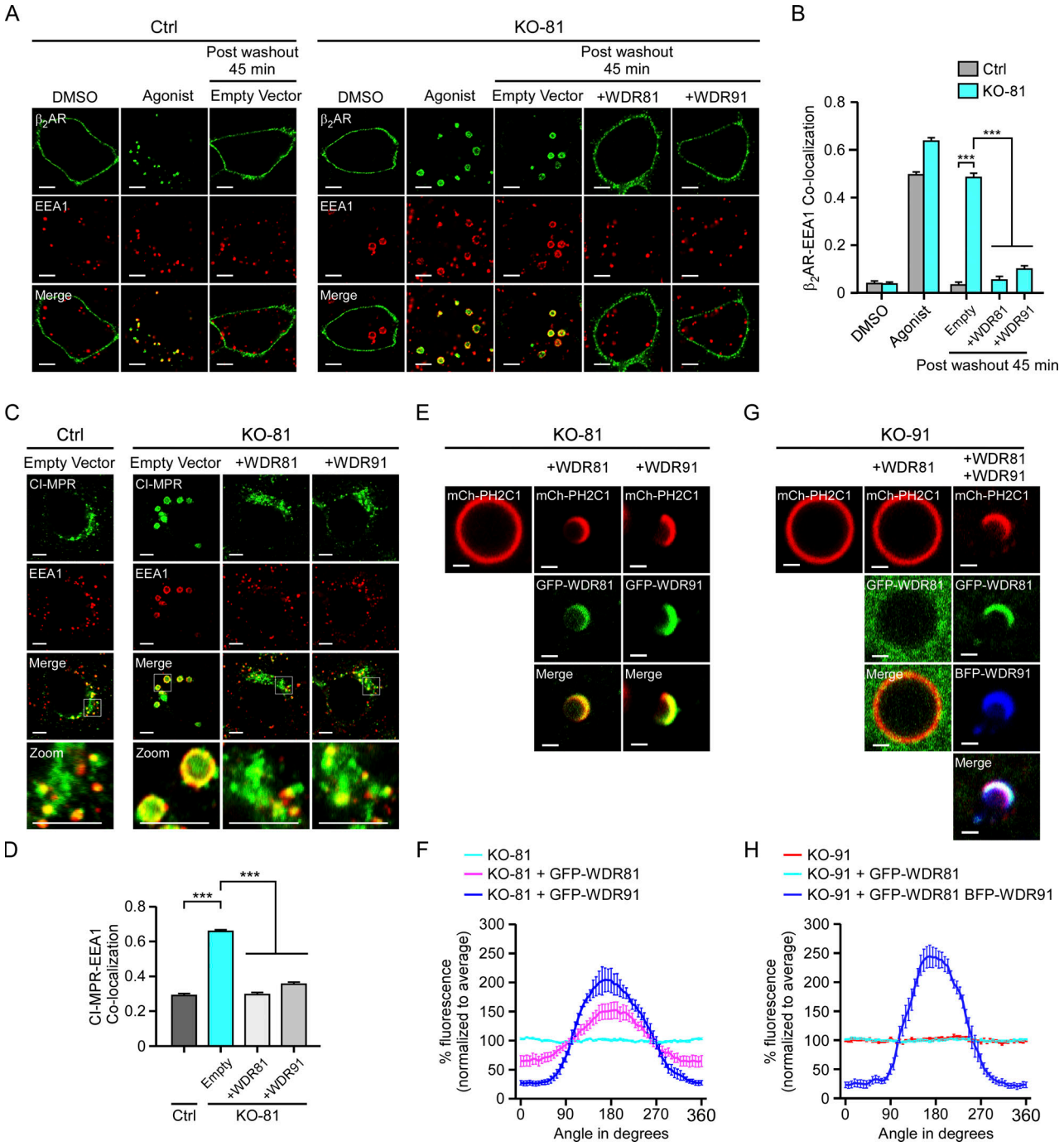

Figure 7. **WDR81 acts through WDR91 to affect endosomal subdomain formation and recycling of membrane receptors. (A)** Representative images from a visual trafficking assay of Flag-β_2AR–expressing Ctrl HeLa cells, KO-81 HeLa cells, and KO-81 cells transfected with empty, Myc-WDR81–, or Myc-WDR91–expressing vectors. 24 h after transfection, the cells were fixed under the indicated conditions including no treatment (DMSO), isoproterenol perfusion for 30 min (Agonist), and isoproterenol perfusion for 30 min followed by washout and further incubation for 45 min (Post washout 45 min). Bars, 5 µm. **(B)** Quantification of β_2AR-EEA1 co-localization for the indicated treatments as shown in A. The y-axis shows the value of Pearson's correlation coefficient. *n* = 48 cells (Ctrl, DMSO); *n* = 48 cells (KO-81, DMSO); *n* = 40 cells (Ctrl, Agonist); *n* = 53 cells (KO-81, Agonist); *n* = 44 cells (Ctrl, Post washout 45 min); *n* = 46 cells (KO-81, empty, Post washout 45 min); *n* = 44 cells (KO-81 + WDR81, Post washout 45 min); *n* = 50 cells (KO-81 + WDR91, Post washout 45 min). **(C)** Co-immunostaining of endogenous CI-MPR in Ctrl and KO-81 HeLa cells transfected with empty, Myc-WDR81–, or Myc-WDR91–expressing vectors. Zoom images show magnified frames in the merged images. 24 h after transfection, the cells were fixed and stained with CI-MPR and EEA1 antibodies. Bars, 5 µm. **(D)** Quantification of the co-localization of CI-MPR with EEA1 as shown in C. *n* = 49 cells (Ctrl); *n* = 47 cells (KO-81, empty); *n* = 46 cells (KO-81 + WDR81); *n* = 49 cells (KO-81 + WDR91). Co-localization was quantified according to Pearson's correlation coefficient. **(E)** Representative images of endosomal mCh-PH2C1 in KO-81 cells without or with ectopic expression of GFP-WDR81 and GFP-WDR91. Bars, 1 µm. **(F)** Measurement of mCh-PH2C1 fluorescence intensity in a clockwise direction along the endosomal membrane as shown in E. *n* = 12 endosomes (KO-81); *n* = 13 endosomes (KO-81 + GFP-WDR81); *n* = 11 endosomes (KO-81 + GFP-WDR91). The profiles of endosomes were obtained and normalized to achieve the average endosomal mCh-PH2C1 fluorescence intensity

(mean ± SEM). **(G)** Representative images of endosomal mCh-PH2C1 in KO-91 cells without or with expression of GFP-WDR81, and GFP-WDR81 together with BFP-WDR91. Bars, 1 µm. **(H)** Measurement of mCh-PH2C1 fluorescence intensity in a clockwise direction along the endosomal membrane as shown in G. *n* = 10 endosomes (KO-91); *n* = 11 endosomes (KO-91 + GFP-WDR81); *n* = 11 endosomes (KO-91 + GFP-WDR81 + BFP-WDR91). The profiles of endosomes were obtained and normalized to achieve the average endosomal mCh-PH2C1 fluorescence intensity (mean ± SEM). For all quantifications, error bars represent SEM. Data are from three independent experiments. Statistical analyses were performed with one-way ANOVA with Tukey's post hoc test. ***, P < 0.001. NS, P > 0.05.

subdomains. In addition, we examined the requirement for retromer components in endosomal recruitment of FAM21/WASH in KO-91 cells. VPS35 siRNA greatly reduced FAM21 association with Rab7-positive endosomes (Fig. 8, F and G), as reported previously (Harbour et al., 2012; Jia et al., 2012). siRNA of SNX27 also significantly decreased FAM21 intensity on Rab7-positive endosomes (Fig. 8, F and G). Collectively, these results suggest that VPS35 and SNX27 promote endosomal recruitment of FAM21 independently of WDR91.

Depletion of WASH complex was shown to induce elongated retromer-decorated membrane tubules (Derivery et al., 2009; Gomez and Billadeau, 2009). To further determine the effect of WDR91 on WASH in retromer-mediated recycling, we investigated the requirement for WDR91 in formation of retromer tubules in cells treated with siRNA against the WASH subunit KIAA1033 (Fig. 8 H). In Ctrl cells, KIAA1033 siRNA induced elongated membrane tubules decorated with SNX27 or VPS35 (Fig. 8 I), consistent with previous reports (Derivery et al., 2009; Gomez and Billadeau, 2009). In contrast, KIAA1033 siRNA seldom induced such tubules in KO-91 cells (Fig. 8 J). These findings suggest that WDR91 probably functions upstream of the WASH complex in retromer-mediated recycling, with WDR91 and WASH being required for formation and release of retromer tubules, respectively.

Discussion

In this study, we identified WDR91 as an essential regulator of endosomal recycling by retromer in mammalian cells. Like other retromer-associated proteins such as TBC1D5 and the WASH complex, WDR91 is not conserved in yeast. Loss of WDR91 led to impairment of both endosome-plasma membrane and endosome-TGN recycling of membrane proteins. Our findings revealed that WDR91 is not required for endosomal recruitment of retromer components, including SNX-BAR proteins, SNX3, SNX27, and VPS35. WDR91 is also dispensable for endosomal recruitment of FAM21/WASH. Instead, loss of WDR91 impaired the enrichment of active Rab7, SNXs, and VPS35 to specific endosomal subdomains, leading to failure of formation of SNX-retromer tubules. Reinforced expression of WDR91 in KO-91 cells re-enriched and restricted active Rab7, SNX-BAR proteins, SNX3, SNX27, and VPS35 to WDR91-specific subdomains on the endosome, where retromer tubules are generated and ultimately released. Taken together, these results suggest that WDR91 plays an indispensable role in formation of the endosomal retrieval subdomain required for retromer-mediated cargo recycling. Mechanistically, WDR91 interacts with the PX domain of SNX-BAR proteins, SNX3, and SNX27, which promotes the interaction between Rab7 and SNXs on endosomes. While a previous proteomic analysis failed to detect the association of WDR91 with retromer (McGough et al., 2014), our data in this study clearly indicate that WDR91 also interacts with VPS35, hence promoting VPS35 interaction with Rab7. The WASH component FAM21 is recruited to endosomes by VPS35, a process which is facilitated by SNX27. However, WDR91 is required for specific co-localization of FAM21 to the endosomal retrieval subdomain with active Rab7 and retromer components. Thus, as a Rab7 effector, WDR91 cooperates with Rab7, the major components of SNX-retromer, and regulators of endosomal actin organization to form the endosomal retrieval subdomain. Together with previous reports that SNX-retromer can generate membrane tubules in vitro (Kovtun et al., 2018; Leneva et al., 2021), our findings suggest that WDR91-dependent enrichment of Rab7 and SNX-retromer at endosomal retrieval subdomains plays an important role in retromer-mediated membrane tubulation (Fig. 9).

Retromer-dependent endosomal cargo retrieval and recycling is intimately coupled with early-to-late endosome conversion. As a Rab7 effector, WDR91 is recruited to endosomes by active Rab7. WDR91 then inhibits endosomal synthesis of PtdIns3P. WDR91 thus couples Rab switching to PtdIns3P downregulation to facilitate endosome conversion (Liu et al., 2016; Liu et al., 2017). Because endosomal PtdIns3P elevation may affect normal endosomal functions, it is important to be aware that the effects of WDR91 depletion may indirectly result from PtdIns3P upregulation as well as from the direct requirement for WDR91 in retromer-mediated endosomal recycling. Our findings in this study suggest that WDR91 plays a central role in coordinating retromer-dependent retrieval and recycling of endosomal cargoes with endosome maturation. In the absence of WDR91, endosomal PtdIns3P is elevated (Liu et al., 2016; Liu et al., 2017). This probably enhances endosomal trapping of SNX-BAR proteins and SNX3, whose endosomal association is dependent on PtdIns3P (Fig. S2). The enrichment of these SNX proteins on the endosomal retrieval subdomain should require the presence of WDR91, which physically interacts with SNX proteins through the PX domain. It is likely that SNX-BAR– and SNX3-retromer–mediated endosome-TGN recycling of membrane receptors (e.g., CI-MPR, Wntless) occurs at an earlier stage of endosome conversion, concomitant with the WDR91-facilitated reduction in PtdIns3P. Unlike SNX-BAR proteins, endosomal association of SNX27 is not entirely dependent on PtdIns3P, and SNX27 remains associated with Rab7-positive endosomes even when endosomal PtdIns3P is diminished (Fig. 3, A–D, and Fig. S1, A–D). Thus, SNX27-retromer–mediated endosome-plasma membrane recycling of cargoes probably occurs throughout the entire endosome conversion process as well as on late endosomes that are characterized by Rab7 and low

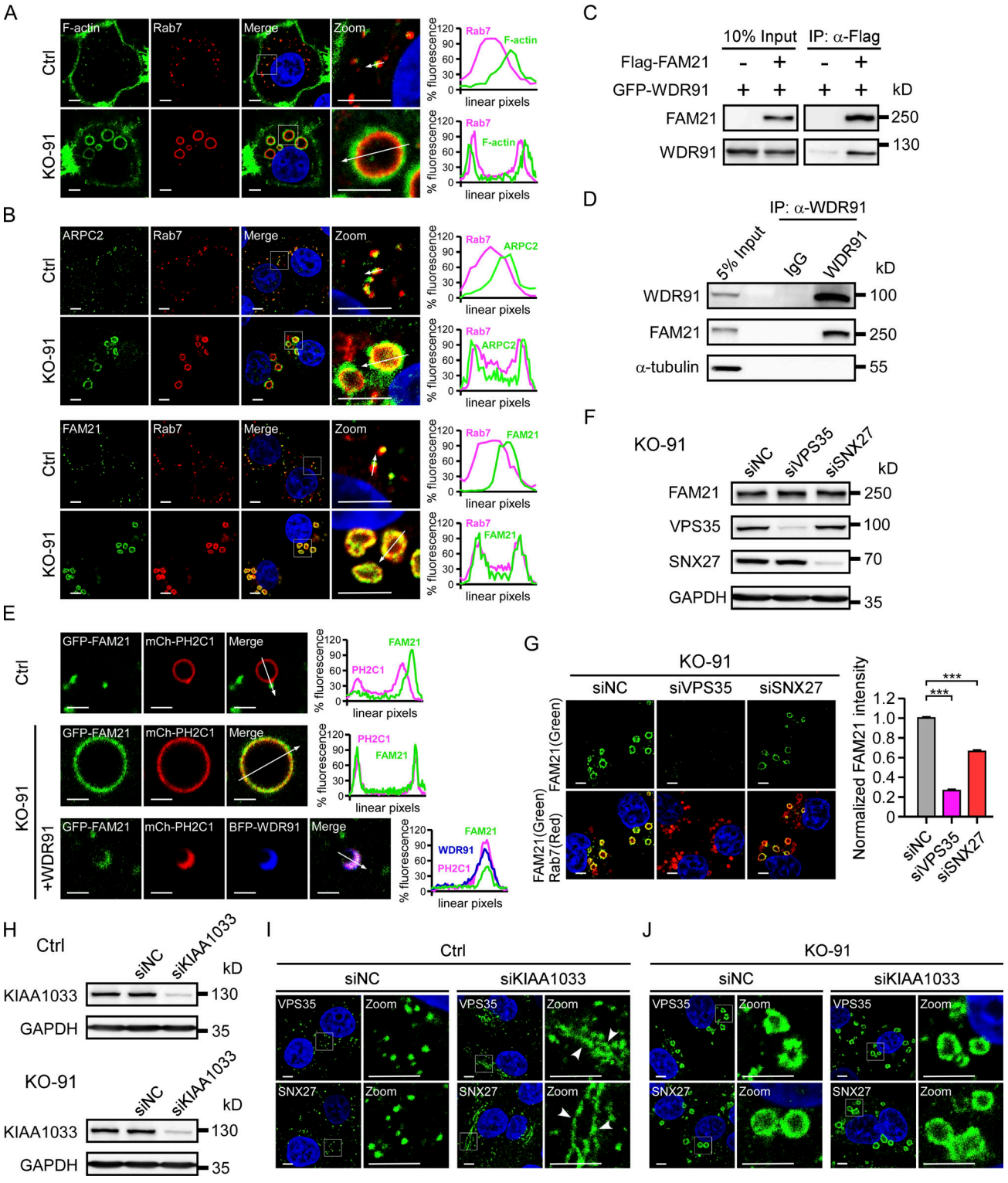

Figure 8. **WDR91 coordinates with the FAM21-containing WASH complex to organize the actin network for formation of endosomal retrieval subdomains. (A)** Co-localization of phalloidin-stained F-actin with Rab7 in Ctrl and KO-91 cells. Zoom images show magnified frames in the merged images. Quantifications of linear pixel fluorescence of F-actin (green) and Rab7 (magenta) along the arrows across the endosomes in the zoom images are shown on the right. Bars, 5 µm. **(B)** Co-immunostaining of Rab7 with endogenous ARPC2 (top), and FAM21 (bottom) in Ctrl and KO-91 cells. Zoom images show magnified frames in the merged images. Quantifications of linear pixel fluorescence of Rab7 (magenta), ARPC2 (green), or FAM21 (green) along the arrows across the endosomes in the zoom images are shown on the right. Bars, 5 µm. **(C)** Co-IP of Flag-FAM21 with GFP-WDR91. IPs were performed with anti-Flag antibody resin and immunoblotted using Flag and GFP antibodies. **(D)** Co-IP of endogenous FAM21 with WDR91 in control HeLa cells. IP was performed with WDR91 antibody and precipitated proteins were detected with antibodies against the indicated proteins. **(E)** Co-localization of GFP-FAM21 with mCh-PH2C1 in Ctrl, KO-91 cells, and KO-91 cells re-expressing BFP-WDR91. Bars, 2 µm. Quantification of linear pixel fluorescence of GFP-FAM21 (green), mCh-PH2C1 (magenta),

and BFP-WDR91 (blue) along the arrows across the endosomes in the merge images are shown on the right. **(F)** Immunoblotting of endogenous FAM21, VPS35, and SNX27 in KO-91 cells treated with negative control siRNA (siNC), VPS35 siRNA (siVPS35), and SNX27 siRNA (siSNX27). **(G)** Co-immunostaining of endogenous FAM21 with Rab7 in KO-91 cells treated with siNC, siVPS35, and siSNX27. Bars, 5 µm. Quantification of endogenous FAM21 intensity on endosomes is shown on the right. n = 50 cells (siNC); n = 50 cells (siVPS35); n = 48 cells (siSNX27). Statistical analyses were performed with the Kruskal–Wallis test. ***, $P < 0.001$. **(H)** Immunoblotting of endogenous KIAA1033 in Ctrl (top) and KO-91 (bottom) cells treated with siNC and KIAA1033 siRNA (siKIAA1033). **(I)** Immunostaining of endogenous VPS35 (top) and SNX27 (bottom) in Ctrl HeLa cells treated with siNC and siKIAA1033. Zoom images show magnified frames in the left column in each group. Membrane tubules are indicated with arrowheads. Bars, 5 µm. **(J)** Immunostaining of endogenous VPS35 (top) and SNX27 (bottom) in KO-91 cells treated with siNC and siKIAA1033. Zoom images show magnified frames in the left column in each group. Bars, 5 µm. Source data are available for this figure: SourceData F8.

PtdIns3P levels. Rab7-dependent endosomal recruitment of WDR91 not only inhibits endosomal PtdIns3P synthesis to allow endosome conversion but also enables the formation of the endosomal retrieval subdomain that is shared by SNX-BAR-, SNX3-, and SNX27-retromer (Burd and Cullen, 2014; McNally and Cullen, 2018). In addition, SNX-BAR proteins were found to form an evolutionarily conserved coat complex, ESCPE-1 (Endosomal SNX–BAR sorting complex for promoting exit 1), which mediates CSC-independent retrograde transport (Simonetti et al., 2019; Yong et al., 2020). Thus, WDR91-dependent formation of retrieval subdomains should also play an important role in the function of ESCPE-1.

The discovery that WDR91 specifies the endosomal retrieval subdomain suggests that WDR91 plays a central role in fate determination of endosomal cargoes. Our recent work revealed that WDR91 competes against the HOPS subunit VPS41 for binding with Rab7, thereby preventing HOPS assembly on late endosomes and hence their fusion with immature endosomes (Xing et al., 2021). Altogether, these findings suggest that WDR91 distinguishes endosomal retrieval subdomains from endosome-lysosome fusion domains. In addition, several lines of evidence demonstrated that the localization of Rab7 on late endosomes and lysosomes is tightly controlled by the retromer–TBC1D5 axis (Jimenez-Orgaz et al., 2018; Kvainickas et al., 2019). These findings, together with our discoveries that WDR91 enriches active Rab7 and SNX-retromer at retrieval subdomains, suggest that the spatial restriction of Rab7 serves as an important basis for proper endosomal functions.

Notably, the retriever complex, which consists of DSCR3-C16orf62-VPS29 heterotrimer and the cargo adaptor SNX17, shares structural and compositional similarities with retromer complex (McNally and Cullen, 2018; McNally et al., 2017). Although retriever and retromer mediate recycling of different cargoes, they were found to localize to the same endosomal retrieval subdomain (McNally and Cullen, 2018; McNally et al., 2017). Interestingly, both retriever- and retromer-dependent pathways were found to be regulated by the CCC (COMMD/CCDC22/CCDC93) complex, which controls PtdIns3P levels on

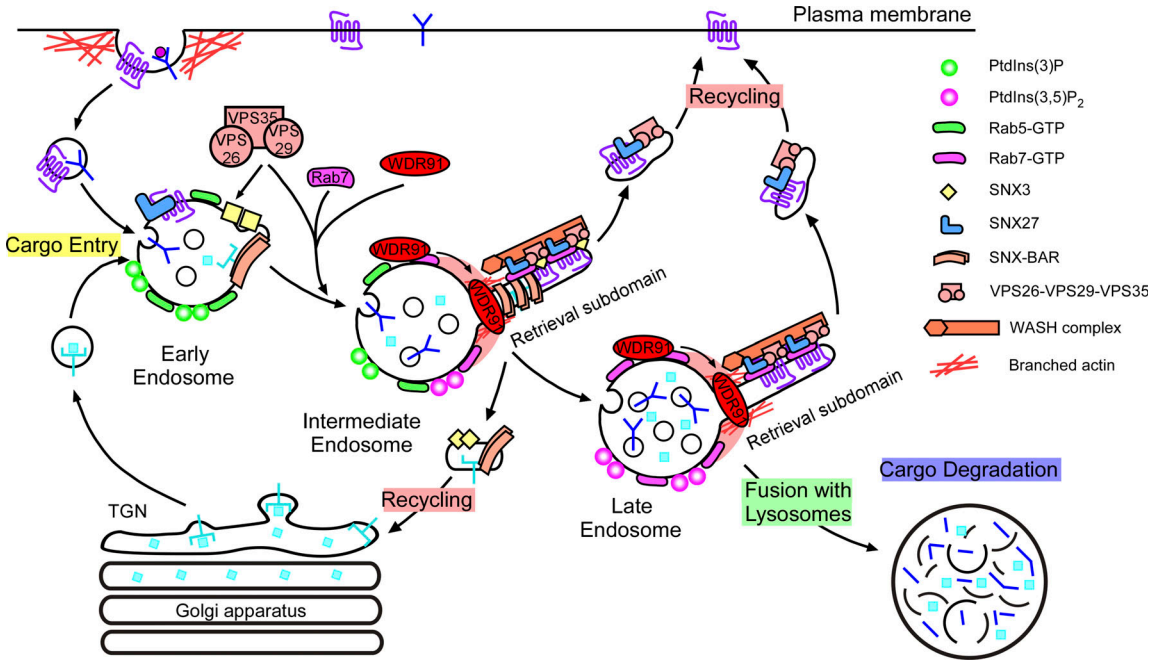

Figure 9. **Schematic summary of WDR91 function in retromer-dependent recycling.** SNX-retromer–mediated endosomal recycling occurs concomitantly with endosome conversion in the endosome–lysosome pathway. During the early-to-late endosome conversion, the active Rab7 recruits WDR91 to endosomes, where WDR91 inhibits endosomal PtdIns3P synthesis to facilitate endosome maturation. WDR91 promotes the interaction of Rab7 with SNX-retromer components, and interacts with the WASH complex on endosomes, thereby establishing the endosomal retrieval domain required for generation and release of retromer tubules.

endosomal membranes through the myotubularin-related protein-2 (MTMR2) lipid phosphatase (Singla et al., 2019). The SNX17-Retriever-CCC-WASH pathway also coordinates with the endosomal switch of PtdIns3P to PtdIns(3,5)P_2 (Giridharan et al., 2022). These findings suggest that, similar to retromer, the function of retriever is coupled with early-to-late endosome conversion. It will be interesting to investigate whether and how WDR91 is involved in retriever-dependent endosomal retrieval and recycling.

Materials and methods

Cell culture and transfection

HeLa or HEK293 cells were maintained in DMEM (Gibco) supplemented with 10% FBS (Biological Industries), 100 U/ml penicillin, and 100 mg/ml streptomycin (HyClone) in a water-saturated 5% CO_2 incubator at 37°C. Cells were tested for mycoplasma contamination using DAPI staining, and the test results were negative. Transfections were performed with Lipofectamine 2000 (Invitrogen) according to the manufacturer's instructions.

Antibodies and reagents

The commercial antibodies and reagents used in this study are listed in Table S1. GFP antibodies were generated in mice and rabbits by injecting purified recombinant His_6-GFP. Rab7 antibody was generated in mice by injecting purified GST-Rab7. WDR91 antibody was generated in mice by injecting purified GST-WDR91(406–730).

Expression vectors

Mammalian and bacterial expression vectors were constructed using standard protocols and are listed in Table S2. mCherry-CD63-expressing vector was provided by H. Zhang (Institute of Biophysics, Chinese Academy of Sciences, Beijing, China). pHluorin-GluA2 was provided by W. Guo (Institute of Genetics and Developmental Biology, Chinese Academy of Sciences, Beijing, China).

siRNAs

RNA oligonucleotides used for siRNA were purchased from GenePharma Co., Ltd. The sequences were as follows: NC, 5′-UUCUCCGAACGUGUCACGUTT-3′, SNX27, 5′-CCAGGUAAUUGCAUUUGAATT-3′, VPS35, 5′-AAAUACCAGUUGACACUUATT-3′, KIAA1033-1, 5′-GCCCUCUAUAUCAGUAACATT-3′, KIAA1033-2, 5′-GAGCUGUCUUCCCAAUUUATT-3′, KIAA1033-3, 5′-GGCCAAAGAAUAUACAUCUTT-3′.

Cells grown in 6-well plates or glass-bottom dishes were transfected with 100 pmol RNA oligonucleotides twice at an interval of 24 h using Lipofectamine 2000 (Invitrogen). Cells were harvested for further experiments 72 h after the first transfection.

Dissection, culture, and transfection of primary hippocampal neurons

Hippocampal neurons were isolated from newborn *Wdr91*$^{+/+}$ or *Wdr91*$^{-/-}$ mice. Hippocampi were microdissected in ice-cold HBSS (Gibco) followed by digestion in 0.05% trypsin-EDTA (Invitrogen) for 15 min at RT (~25°C). The enzymatic reaction was terminated in DMEM (Gibco) supplemented with 10% FBS (Biological Industries). After centrifugation, the cell pellet was re-suspended in DMEM supplemented with 10% FBS and plated on poly-D-lysine–coated 35-mm glass-bottom dishes (Cellvis). 6 h later, neurons were cultured in Neurobasal medium (Gibco) supplemented with 2% B27, 1% glutaMAX, and 1% antibiotics in a water-saturated 5% CO_2 incubator at 37°C. Neurons were transfected 5 d after isolation. 2 µg of total DNA and 3 µl of Lipofectamine 2000 reagent that was diluted in Opti-MEM medium (Gibco) were used in a 35-mm dish. 48 h after the transfection, the neurons were subjected to further analysis.

pH-GluA2 imaging

Hippocampal neurons from *Wdr91*$^{+/+}$ or *Wdr91*$^{-/-}$ P0 mice were transfected with plasmids on day in vitro 5 and imaging experiments were performed 48 h after transfection. On the day of the imaging experiment, neurons were continuously perfused with recording buffer (25 mM Hepes, pH 7.5, 120 mM NaCl, 5 mM KCl, 2.5 mM $CaCl_2$, 1.5 mM $MgCl_2$, 30 mM glucose, and 1 mM Tetrodotoxin). Images were collected for 10 min to establish a baseline fluorescence (F_0) of pH-GluA2 prior to glutamate treatment. Glutamate (20 µM) was added to the recording buffer and maintained for 5 min, neurons were then continuously perfused for 65 min with fresh recording buffer. The change of pH-GluA2 fluorescence was monitored using an inverted confocal microscope system (FV1000; IX81; Olympus) coupled with a camera (FV10-SPD; Olympus) and a 60× 1.42 NA oil objective. pHluorin was imaged with 488-nm excitation and images were acquired at a rate of 1 image/5 min. All images were processed and analyzed with viewer software (FV10-ASW 4.0a; Olympus) and ImageJ software (National Institutes of Health).

β_2AR recycling assays

HeLa cells were plated in glass-bottom dishes (Cellvis) and transfected with vectors expressing Flag-β_2AR. 24 h after transfection, the cells were incubated with complete medium (DMEM supplemented with 10% FBS, 100 U/ml penicillin, and 100 mg/ml streptomycin) in the presence of rabbit anti-Flag antibody (2 µg/ml) for 25 min at 37°C to selectively label Flag-β_2AR present on the plasma membrane. To detect internalized receptors, cells were subsequently incubated with 10 µM isoproterenol (Sigma-Aldrich) for 30 min and then either fixed or washed and further incubated in complete medium for 30/45/60 min to allow for recycling. Cells were fixed with 4% PFA freshly dissolved in PBS and processed for immunostaining.

Quantitative analysis of retromer tubules

HeLa cells were plated in glass-bottom dishes (Cellvis) and transfected with vectors expressing SNX27-GFP or VPS35-GFP with 2×FYVE-mCh or mCh-CD63. 24 h after transfection, cells were imaged for 10 min at 5-s intervals with an inverted confocal microscope system (LSM880; Zeiss) coupled with a camera using a 100× 1.42 NA oil objective. SNX27-decorated tubules were recognized in the GFP excitation channel, and the mCherry excitation channel was recorded simultaneously to mark the position of endosomes. A tubulation event is defined as the

process from budding to release of a long tubule (≥2 µm) on an endosome. The number of tubulation events was analyzed in ≥15 cells for each group.

Immunostaining and confocal microscopy

Cells were fixed with ice-cold 4% PFA for 20 min followed by permeabilization with 0.3% Triton X-100 for 10 min. After extensive washing with PBS, cells were incubated in blocking buffer (5% BSA, 0.1% TritonX-100, and PBS) for 1 h at RT and then incubated with primary antibodies in reaction buffer (1% BSA, 0.1% TritonX-100, and PBS) at 4°C overnight. Cells were washed extensively again and incubated with Alexa Fluor 488–, Alexa Fluor 568–, or Alexa Fluor 647–conjugated secondary antibodies in reaction buffer for 1 h at RT. After another round of extensive washing, cells were stained with DAPI (Sigma-Aldrich) for 5 min if nuclear staining was needed.

All samples were imaged with an inverted confocal microscope system (LSM880; Zeiss) coupled with a camera using a 100× 1.42 NA oil objective. Excitation was achieved using 405-, 488-, 560-, and 633-nm lasers. All images were acquired at RT and processed with Zen software (Blue edition; Zeiss). The Pearson's correlation coefficient between the channels of interest was used to determine co-localizations. Fluorescent intensity of the endosomal subdomains was measured along an arrow across the subdomain and the endosome, and the pixel values were obtained with the Profile function.

Western blotting and IPs

Cells were lysed in ice-cold RIPA buffer (25 mM Tris-HCl, pH 7.5, 100 mM NaCl, 1% Triton X-100, 0.5% sodium deoxycholate, 0.1% SDS, and 1 mM PMSF) containing Complete Protease Inhibitor Cocktail (Roche). Cell lysates were cleared by centrifugation at 12,000 rpm for 10 min at 4°C, and the protein concentration of supernatants was determined using the Bradford assay. Equal protein loads were separated by SDS-PAGE, transferred to nitrocellulose membrane, and probed with the indicated antibodies. GAPDH was used as the loading control. Blots were acquired with the ECL chemiluminescent detection reagents (GE Healthcare and Thermo Fisher Scientific) and imaged with the Smartchemi machine (Sage Creation).

To examine interactions of proteins tagged with different epitopes, the corresponding expression vectors were co-expressed in HEK293 cells. After 48 h, cells were lysed in ice-cold co-IP buffer (25 mM Tris-HCl, pH 7.5, 100 mM NaCl, 1% NP-40, 1 mM PMSF, and 1% glycerol) containing Complete Protease Inhibitor Cocktail (Roche). Cell lysates were spun at 5,000 rpm for 10 min at 4°C, and the supernatants were incubated with Flag antibody (M2)-conjugated beads (Sigma-Aldrich) or GFP-trap beads (ChromoTek) overnight at 4°C. The beads were centrifuged and washed three times with wash buffer (25 mM Tris-HCl, pH 7.5, 150 mM NaCl, 0.1% NP-40 and 1 mM PMSF), and the precipitated proteins were detected by Western blotting. For GFP-based immunoprecipitations, HeLa cells were washed with cold PBS and lysed 24 h after transfection in ice-cold IP buffer (25 mM Tris-HCl, pH 7.5, 50 mM NaCl, 0.1% NP-40, 1 mM PMSF, and 1% glycerol, complete protease inhibitor cocktail) and the supernatants were mixed with GFP-trap beads (ChromoTek). For IP of endogenous proteins, HeLa cells were washed with cold PBS prior to lysis (25 mM Tris-HCl, pH 7.5, 50 mM NaCl, 0.1% NP-40, 1 mM PMSF, and 1% glycerol, complete protease inhibitor cocktail). Cell lysates were spun at 5,000 rpm for 10 min at 4°C, and the supernatants were then incubated with either mouse IgG or mouse Rab7/WDR91 antibodies overnight at 4°C on a roller. Pre-washed protein A beads (GE Healthcare) were added to the lysates and were further incubated for 4 h at 4°C on a roller. The beads were centrifuged and washed three times with wash buffer (25 mM Tris-HCl, pH 7.5, 150 mM NaCl, 0.1% NP-40, and 1 mM PMSF), and the precipitated proteins were resolved and detected by Western blotting.

FRAP analysis

FRAP was performed on a confocal microscope (LSM880; Zeiss) equipped with a 100× 1.42 NA oil objective at RT. Defined endosomal subdomains were photobleached by 560-nm laser with 100% power. Images were collected before and after photobleaching and fluorescence intensity was measured by Mean ROI at 1-s intervals. For kinetic analysis, fluorescence recovery curves were plotted against time by setting the intensity before photo-bleaching as 1 and the minimum intensity after photobleaching as 0. Recovery half-times ($t_{1/2}$) were calculated by fitting each curve to a mono-exponential equation.

Recombinant proteins

All recombinant proteins used in this study were expressed in BL21 (Rosetta) bacterial cells induced by 0.4 mM IPTG for 24 h at 18°C and collected by centrifugation. The cell pellet was resuspended in lysis buffer (25 mM Tris-HCl, pH 8.0, 150 mM NaCl, 0.1% NP-40, 10% glycerol, and 1 mM PMSF) and subjected to sonication. The supernatant lysates were incubated with glutathione-Sepharose beads (GE Healthcare) or His_6-binding beads (GE Healthcare) overnight at 4°C to pull down proteins of interest. After extensive washing, the bound proteins were eluted with elution buffer (25 mM Tris-HCl, pH 7.5, 300 mM NaCl, and 200 mM imidazole for His_6-tagged proteins, or 25 mM Tris-HCl, pH 7.5, 300 mM NaCl, and 10 mM reduced Glutathione for GST-tagged proteins).

GST pull-down assays

Purified GST-tagged proteins (2.5 µg) were immobilized on glutathione-Sepharose beads and incubated with His_6-tagged proteins in binding buffer (25 mM Tris-HCl, pH 7.5, 100 mM NaCl, 0.1% NP-40, 10 mM DTT, 1 mM PMSF, and protease inhibitor cocktail) at 4°C overnight. After extensive washing with wash buffer (25 mM Tris-HCl, pH 7.5, 150 mM NaCl, 0.1% NP-40, and 1 mM PMSF), bound proteins were resolved by SDS-PAGE and detected by Western blotting.

Statistical analysis

Data were analyzed in Prism (GraphPad Software) or Origin (OriginPro Software) to generate curves or bar graphs. All error bars represent SEM. Data distribution was tested for normality using a D'Agostino & Pearson omnibus K2 test. The two-tailed unpaired *t* test was used for statistical comparisons of two

groups of samples that comply with Gaussian distribution. The Mann-Whitney *U*-test was performed for statistical comparisons of two groups of samples that do not follow Gaussian distribution. One-way ANOVA with Tukey's post hoc test and the Kruskal–Wallis test were used for statistical comparisons of three or more groups of samples. *, $P < 0.05$; **, $P < 0.01$; ***, $P < 0.001$. $P > 0.05$ was considered not significant.

Online supplemental material

Fig. S1 characterizes endosomal association of SNX27 and VPS35. Fig. S2 characterizes endosomal localization of endogenous SNX6, SNX2, and SNX3. Fig. S3 analyzes the rescuing effect of wild-type and mutant WDR91 on defective AMPA receptor recycling. Fig. S4 characterizes the interaction of WDR91 with SNX27, SNX-BAR proteins, SNX3, and their PX domains and VPS35. Fig. S5 characterizes endosomal localization of endogenous ARPC2 and FAM21, and protein interaction of WDR91, ARP2, ARP3, FAM21, SNX27, and VPS35. Table S1 lists the commercial antibodies and reagents used in the study. Table S2 lists the expression vectors used in the study. Videos 1 and 2 show time-lapse monitoring of SNX27-GFP on 2×FYVE-mCh–positive or CD63-mCh–positive endosomes in Ctrl and KO-91 HeLa cells. Video 3 shows time-lapse monitoring of SNX27-GFP and mCh-WDR91 in Ctrl HeLa cells. Video 4 shows time-lapse monitoring of VPS35-GFP and mCh-WDR91 in Ctrl HeLa cells.

Acknowledgments

We thank W. Guo (Institute of Genetic and Developmental Biology, China Academy of Sciences), R. Xing (Institute of Genetic and Developmental Biology, China Academy of Sciences), and M. Yang (Yunnan University) for technical assistance with neuronal experiments, and I. Hanson for proofreading of the manuscript.

This work was supported by grants from the National Basic Research Program of China (2017YFA0503403), the National Science Foundation of China (31730053 and 91954204 to C. Yang; 31900500 to N. Liu), and Yunnan Province Science and Technology Department (202001BB050077). C. Yang is supported by Program of Yunnan Province Leading Talents in Science and Technology.

The authors declare no competing financial interests.

Author contributions: C. Yang and N. Liu conceived and designed the research. C. Yang supervised the research. N. Liu did most of the experiments and analyzed the data. K. Liu contributed to the experiments and materials. N. Liu and C. Yang prepared the manuscript with feedback from all authors.

Submitted: 4 March 2022
Revised: 4 August 2022
Accepted: 19 September 2022

References

Arighi, C.N., L.M. Hartnell, R.C. Aguilar, C.R. Haft, and J.S. Bonifacino. 2004. Role of the mammalian retromer in sorting of the cation-independent mannose 6-phosphate receptor. *J. Cell Biol.* 165:123–133. https://doi.org/10.1083/jcb.200312055

Ashby, M.C., S.A. De La Rue, G.S. Ralph, J. Uney, G.L. Collingridge, and J.M. Henley. 2004. Removal of AMPA receptors (AMPARs) from synapses is preceded by transient endocytosis of extrasynaptic AMPARs. *J. Neurosci.* 24:5172–5176. https://doi.org/10.1523/JNEUROSCI.1042-04.2004

Bonifacino, J.S., and R. Rojas. 2006. Retrograde transport from endosomes to the trans-Golgi network. *Nat. Rev. Mol. Cell Biol.* 7:568–579. https://doi.org/10.1038/nrm1985

Burd, C., and P.J. Cullen. 2014. Retromer: A master conductor of endosome sorting. *Cold Spring Harbor Perspect. Biol.* 6:a016774. https://doi.org/10.1101/cshperspect.a016774

Burda, P., S.M. Padilla, S. Sarkar, and S.D. Emr. 2002. Retromer function in endosome-to-Golgi retrograde transport is regulated by the yeast Vps34 PtdIns 3-kinase. *J. Cell Sci.* 115:3889–3900. https://doi.org/10.1242/jcs.00090

Cantalupo, G., P. Alifano, V. Roberti, C.B. Bruni, and C. Bucci. 2001. Rab-interacting lysosomal protein (RILP): The Rab7 effector required for transport to lysosomes. *EMBO J.* 20:683–693. https://doi.org/10.1093/emboj/20.4.683

Carlton, J.G., M.V. Bujny, B.J. Peter, V.M. Oorschot, A. Rutherford, R.S. Arkell, J. Klumperman, H.T. McMahon, and P.J. Cullen. 2005. Sorting nexin-2 is associated with tubular elements of the early endosome, but is not essential for retromer-mediated endosome-to-TGN transport. *J. Cell Sci.* 118:4527–4539. https://doi.org/10.1242/jcs.02568

Chandra, M., Y.K. Chin, C. Mas, J.R. Feathers, B. Paul, S. Datta, K.E. Chen, X. Jia, Z. Yang, S.J. Norwood, et al. 2019. Classification of the human phox homology (PX) domains based on their phosphoinositide binding specificities. *Nat. Commun.* 10:1528. https://doi.org/10.1038/s41467-019-09355-y

Cozier, G.E., J. Carlton, A.H. McGregor, P.A. Gleeson, R.D. Teasdale, H. Mellor, and P.J. Cullen. 2002. The phox homology (PX) domain-dependent, 3-phosphoinositide-mediated association of sorting nexin-1 with an early sorting endosomal compartment is required for its ability to regulate epidermal growth factor receptor degradation. *J. Biol. Chem.* 277:48730–48736. https://doi.org/10.1074/jbc.M206986200

Cullen, P.J., and H.C. Korswagen. 2011. Sorting nexins provide diversity for retromer-dependent trafficking events. *Nat. Cell Biol.* 14:29–37. https://doi.org/10.1038/ncb2374

Cullen, P.J., and F. Steinberg. 2018. To degrade or not to degrade: Mechanisms and significance of endocytic recycling. *Nat. Rev. Mol. Cell Biol.* 19:679–696. https://doi.org/10.1038/s41580-018-0053-7

Derivery, E., C. Sousa, J.J. Gautier, B. Lombard, D. Loew, and A. Gautreau. 2009. The Arp2/3 activator WASH controls the fission of endosomes through a large multiprotein complex. *Dev. Cell.* 17:712–723. https://doi.org/10.1016/j.devcel.2009.09.010

Giridharan, S.S.P., G. Luo, P. Rivero-Rios, N. Steinfeld, H. Tronchere, A. Singla, E. Burstein, D.D. Billadeau, M.A. Sutton, and L.S. Weisman. 2022. Lipid kinases VPS34 and PIKfyve coordinate a phosphoinositide cascade to regulate retriever-mediated recycling on endosomes. *Elife.* 11:e69709. https://doi.org/10.7554/eLife.69709

Gokool, S., D. Tattersall, J.V. Reddy, and M.N. Seaman. 2007. Identification of a conserved motif required for Vps35p/Vps26p interaction and assembly of the retromer complex. *Biochem. J.* 408:287–295. https://doi.org/10.1042/BJ20070555

Gomez, T.S., and D.D. Billadeau. 2009. A FAM21-containing WASH complex regulates retromer-dependent sorting. *Dev. Cell.* 17:699–711. https://doi.org/10.1016/j.devcel.2009.09.009

Harbour, M.E., S.Y. Breusegem, and M.N.J. Seaman. 2012. Recruitment of the endosomal WASH complex is mediated by the extended "tail" of Fam21 binding to the retromer protein Vps35. *Biochem. J.* 442:209–220. https://doi.org/10.1042/BJ20111761

Harrison, M.S., C.S. Hung, T.T. Liu, R. Christiano, T.C. Walther, and C.G. Burd. 2014. A mechanism for retromer endosomal coat complex assembly with cargo. *Proc. Natl. Acad. Sci. USA.* 111:267–272. https://doi.org/10.1073/pnas.1316482111

Harterink, M., F. Port, M.J. Lorenowicz, I.J. McGough, M. Silhankova, M.C. Betist, J.R.T. van Weering, R.G.H.P. van Heesbeen, T.C. Middelkoop, K. Basler, et al. 2011. A SNX3-dependent retromer pathway mediates retrograde transport of the Wnt sorting receptor Wntless and is required for Wnt secretion. *Nat. Cell Biol.* 13:914–923. https://doi.org/10.1038/ncb2281

Huotari, J., and A. Helenius. 2011. Endosome maturation. *EMBO J.* 30:3481–3500. https://doi.org/10.1038/emboj.2011.286

Jia, D., T.S. Gomez, D.D. Billadeau, and M.K. Rosen. 2012. Multiple repeat elements within the FAM21 tail link the WASH actin regulatory complex to the retromer. *Mol. Biol. Cell.* 23:2352–2361. https://doi.org/10.1091/mbc.E11-12-1059

Jia, D., J.S. Zhang, F. Li, J. Wang, Z. Deng, M.A. White, D.G. Osborne, C. Phillips-Krawczak, T.S. Gomez, H. Li, et al. 2016. Structural and

mechanistic insights into regulation of the retromer coat by TBC1d5. *Nat. Commun.* 7:13305. https://doi.org/10.1038/ncomms13305

Jimenez-Orgaz, A., A. Kvainickas, H. Nagele, J. Denner, S. Eimer, J. Dengjel, and F. Steinberg. 2018. Control of RAB7 activity and localization through the retromer-TBC1D5 complex enables RAB7-dependent mitophagy. *EMBO J.* 37:235–254. https://doi.org/10.15252/embj.201797128

Kendall, A.K., B. Xie, P. Xu, J. Wang, R. Burcham, M.N. Frazier, E. Binshtein, H. Wei, T.R. Graham, T. Nakagawa, and L.P. Jackson. 2020. Mammalian retromer is an adaptable scaffold for cargo sorting from endosomes. *Structure.* 28:393–405.e4. https://doi.org/10.1016/j.str.2020.01.009

Kovtun, O., N. Leneva, Y.S. Bykov, N. Ariotti, R.D. Teasdale, M. Schaffer, B.D. Engel, D.J. Owen, J.A.G. Briggs, and B.M. Collins. 2018. Structure of the membrane-assembled retromer coat determined by cryo-electron tomography. *Nature.* 561:561–564. https://doi.org/10.1038/s41586-018-0526-z

Kvainickas, A., H. Nagele, W. Qi, L. Dokladal, A. Jimenez-Orgaz, L. Stehl, D. Gangurde, Q. Zhao, Z. Hu, J. Dengjel, et al. 2019. Retromer and TBC1D5 maintain late endosomal RAB7 domains to enable amino acid-induced mTORC1 signaling. *J. Cell Biol.* 218:3019–3038. https://doi.org/10.1083/jcb.201812110

Lauffer, B.E., C. Melero, P. Temkin, C. Lei, W. Hong, T. Kortemme, and M. von Zastrow. 2010. SNX27 mediates PDZ-directed sorting from endosomes to the plasma membrane. *J. Cell Biol.* 190:565–574. https://doi.org/10.1083/jcb.201004060

Lee, S., J. Chang, and C. Blackstone. 2016. FAM21 directs SNX27-retromer cargoes to the plasma membrane by preventing transport to the Golgi apparatus. *Nat. Commun.* 7:10939. https://doi.org/10.1038/ncomms10939

Leneva, N., O. Kovtun, D.R. Morado, J.A.G. Briggs, and D.J. Owen. 2021. Architecture and mechanism of metazoan retromer:SNX3 tubular coat assembly. *Sci. Adv.* 7:eabf8598. https://doi.org/10.1126/sciadv.abf8598

Lin, D.T., and R.L. Huganir. 2007. PICK1 and phosphorylation of the glutamate receptor 2 (GluR2) AMPA receptor subunit regulates GluR2 recycling after NMDA receptor-induced internalization. *J. Neurosci.* 27:13903–13908. https://doi.org/10.1523/JNEUROSCI.1750-07.2007

Liu, K., Y. Jian, X. Sun, C. Yang, Z. Gao, Z. Zhang, X. Liu, Y. Li, J. Xu, Y. Jing, et al. 2016. Negative regulation of phosphatidylinositol 3-phosphate levels in early-to-late endosome conversion. *J. Cell Biol.* 212:181–198. https://doi.org/10.1083/jcb.201506081

Liu, K., R. Xing, Y. Jian, Z. Gao, X. Ma, X. Sun, Y. Li, M. Xu, X. Wang, Y. Jing, et al. 2017. WDR91 is a Rab7 effector required for neuronal development. *J. Cell Biol.* 216:3307–3321. https://doi.org/10.1083/jcb.201705151

Lunn, M.L., R. Nassirpour, C. Arrabit, J. Tan, I. McLeod, C.M. Arias, P.E. Sawchenko, J.R. Yates 3rd, and P.A. Slesinger. 2007. A unique sorting nexin regulates trafficking of potassium channels via a PDZ domain interaction. *Nat. Neurosci.* 10:1249–1259. https://doi.org/10.1038/nn1953

McEwan, D.G., D. Popovic, A. Gubas, S. Terawaki, H. Suzuki, D. Stadel, F.P. Coxon, D. Miranda de Stegmann, S. Bhogaraju, K. Maddi, et al. 2015a. PLEKHM1 regulates autophagosome-lysosome fusion through HOPS complex and LC3/GABARAP proteins. *Mol. Cell.* 57:39–54. https://doi.org/10.1016/j.molcel.2014.11.006

McEwan, D.G., B. Richter, B. Claudi, C. Wigge, P. Wild, H. Farhan, K. McGourty, F.P. Coxon, M. Franz-Wachtel, B. Perdu, et al. 2015b. PLEKHM1 regulates Salmonella-containing vacuole biogenesis and infection. *Cell Host Microbe.* 17:58–71. https://doi.org/10.1016/j.chom.2014.11.011

McGough, I.J., F. Steinberg, M. Gallon, A. Yatsu, N. Ohbayashi, K.J. Heesom, M. Fukuda, and P.J. Cullen. 2014. Identification of molecular heterogeneity in SNX27-retromer-mediated endosome-to-plasma-membrane recycling. *J. Cell Sci.* 127:4940–4953. https://doi.org/10.1242/jcs.156299

McNally, K.E., and P.J. Cullen. 2018. Endosomal retrieval of cargo: Retromer is not alone. *Trends Cell Biol.* 28:807–822. https://doi.org/10.1016/j.tcb.2018.06.005

McNally, K.E., R. Faulkner, F. Steinberg, M. Gallon, R. Ghai, D. Pim, P. Langton, N. Pearson, C.M. Danson, H. Nagele, et al. 2017. Retriever is a multiprotein complex for retromer-independent endosomal cargo recycling. *Nat. Cell Biol.* 19:1214–1225. https://doi.org/10.1038/ncb3610

Nakada-Tsukui, K., Y. Saito-Nakano, V. Ali, and T. Nozaki. 2005. A retromerlike complex is a novel Rab7 effector that is involved in the transport of the virulence factor cysteine protease in the enteric protozoan parasite Entamoeba histolytica. *Mol. Biol. Cell.* 16:5294–5303. https://doi.org/10.1091/mbc.e05-04-0283

Norris, A., and B.D. Grant. 2020. Endosomal microdomains: Formation and function. *Curr. Opin. Cell Biol.* 65:86–95. https://doi.org/10.1016/j.ceb.2020.02.018

Norwood, S.J., D.J. Shaw, N.P. Cowieson, D.J. Owen, R.D. Teasdale, and B.M. Collins. 2011. Assembly and solution structure of the core retromer protein complex. *Traffic.* 12:56–71. https://doi.org/10.1111/j.1600-0854.2010.01124.x

Pankiv, S., E.A. Alemu, A. Brech, J.A. Bruun, T. Lamark, A. Overvatn, G. Bjorkoy, and T. Johansen. 2010. FYCO1 is a Rab7 effector that binds to LC3 and PI3P to mediate microtubule plus end-directed vesicle transport. *J. Cell Biol.* 188:253–269. https://doi.org/10.1083/jcb.200907015

Puthenveedu, M.A., B. Lauffer, P. Temkin, R. Vistein, P. Carlton, K. Thorn, J. Taunton, O.D. Weiner, R.G. Parton, and M. von Zastrow. 2010. Sequence-dependent sorting of recycling proteins by actin-stabilized endosomal microdomains. *Cell.* 143:761–773. https://doi.org/10.1016/j.cell.2010.10.003

Rapiteanu, R., L.J. Davis, J.C. Williamson, R.T. Timms, J. Paul Luzio, and P.J. Lehner. 2016. A genetic screen identifies a critical role for the WDR81-WDR91 complex in the trafficking and degradation of tetherin. *Traffic.* 17:940–958. https://doi.org/10.1111/tra.12409

Rink, J., E. Ghigo, Y. Kalaidzidis, and M. Zerial. 2005. Rab conversion as a mechanism of progression from early to late endosomes. *Cell.* 122:735–749. https://doi.org/10.1016/j.cell.2005.06.043

Rojas, R., T. van Vlijmen, G.A. Mardones, Y. Prabhu, A.L. Rojas, S. Mohammed, A.J. Heck, G. Raposo, P. van der Sluijs, and J.S. Bonifacino. 2008. Regulation of retromer recruitment to endosomes by sequential action of Rab5 and Rab7. *J. Cell Biol.* 183:513–526. https://doi.org/10.1083/jcb.200804048

Seaman, M.N. 2004. Cargo-selective endosomal sorting for retrieval to the Golgi requires retromer. *J. Cell Biol.* 165:111–122. https://doi.org/10.1083/jcb.200312034

Seaman, M.N., M.E. Harbour, D. Tattersall, E. Read, and N. Bright. 2009. Membrane recruitment of the cargo-selective retromer subcomplex is catalysed by the small GTPase Rab7 and inhibited by the Rab-GAP TBC1D5. *J. Cell Sci.* 122:2371–2382. https://doi.org/10.1242/jcs.048686

Seaman, M.N., J.M. McCaffery, and S.D. Emr. 1998. A membrane coat complex essential for endosome-to-Golgi retrograde transport in yeast. *J. Cell Biol.* 142:665–681. https://doi.org/10.1083/jcb.142.3.665

Simonetti, B., and P.J. Cullen. 2019. Actin-dependent endosomal receptor recycling. *Curr. Opin. Cell Biol.* 56:22–33. https://doi.org/10.1016/j.ceb.2018.08.006

Simonetti, B., B. Paul, K. Chaudhari, S. Weeratunga, F. Steinberg, M. Gorla, K.J. Heesom, G.J. Bashaw, B.M. Collins, and P.J. Cullen. 2019. Molecular identification of a BAR domain-containing coat complex for endosomal recycling of transmembrane proteins. *Nat. Cell Biol.* 21:1219–1233. https://doi.org/10.1038/s41556-019-0393-3

Singla, A., A. Fedoseienko, S.S.P. Giridharan, B.L. Overlee, A. Lopez, D. Jia, J. Song, K. Huff-Hardy, L. Weisman, E. Burstein, and D.D. Billadeau. 2019. Endosomal PI(3)P regulation by the COMMD/CCDC22/CCDC93 (CCC) complex controls membrane protein recycling. *Nat. Commun.* 10:4271. https://doi.org/10.1038/s41467-019-12221-6

Steinberg, F., M. Gallon, M. Winfield, E.C. Thomas, A.J. Bell, K.J. Heesom, J.M. Tavare, and P.J. Cullen. 2013. A global analysis of SNX27-retromer assembly and cargo specificity reveals a function in glucose and metal ion transport. *Nat. Cell Biol.* 15:461–471. https://doi.org/10.1038/ncb2721

Teasdale, R.D., and B.M. Collins. 2012. Insights into the PX (phox-homology) domain and SNX (sorting nexin) protein families: Structures, functions and roles in disease. *Biochem. J.* 441:39–59. https://doi.org/10.1042/BJ20111226

Temkin, P., B. Lauffer, S. Jager, P. Cimermancic, N.J. Krogan, and M. von Zastrow. 2011. SNX27 mediates retromer tubule entry and endosome-to-plasma membrane trafficking of signalling receptors. *Nat. Cell Biol.* 13:715–721. https://doi.org/10.1038/ncb2252

van Weering, J.R., P. Verkade, and P.J. Cullen. 2012. SNX-BAR-mediated endosome tubulation is co-ordinated with endosome maturation. *Traffic.* 13:94–107. https://doi.org/10.1111/j.1600-0854.2011.01297.x

Xing, R., H. Zhou, Y. Jian, L. Li, M. Wang, N. Liu, Q. Yin, Z. Liang, W. Guo, and C. Yang. 2021. The Rab7 effector WDR91 promotes autophagy-lysosome degradation in neurons by regulating lysosome fusion. *J. Cell Biol.* 220:e202007061. https://doi.org/10.1083/jcb.202007061

Xu, Y., H. Hortsman, L. Seet, S.H. Wong, and W. Hong. 2001. SNX3 regulates endosomal function through its PX-domain-mediated interaction with PtdIns(3)P. *Nat. Cell Biol.* 3:658–666. https://doi.org/10.1038/35083051

Yong, X., L. Zhao, W. Deng, H. Sun, X. Zhou, L. Mao, W. Hu, X. Shen, Q. Sun, D.D. Billadeau, et al. 2020. Mechanism of cargo recognition by retromer-linked SNX-BAR proteins. *PLoS Biol.* 18:e3000631. https://doi.org/10.1371/journal.pbio.3000631

Zhong, Q., C.S. Lazar, H. Tronchère, T. Sato, T. Meerloo, M. Yeo, Z. Songyang, S.D. Emr, and G.N. Gill. 2002. Endosomal localization and function of sorting nexin 1. *Proc. Natl. Acad. Sci. USA.* 99:6767–6772. https://doi.org/10.1073/pnas.092142699

Supplemental material

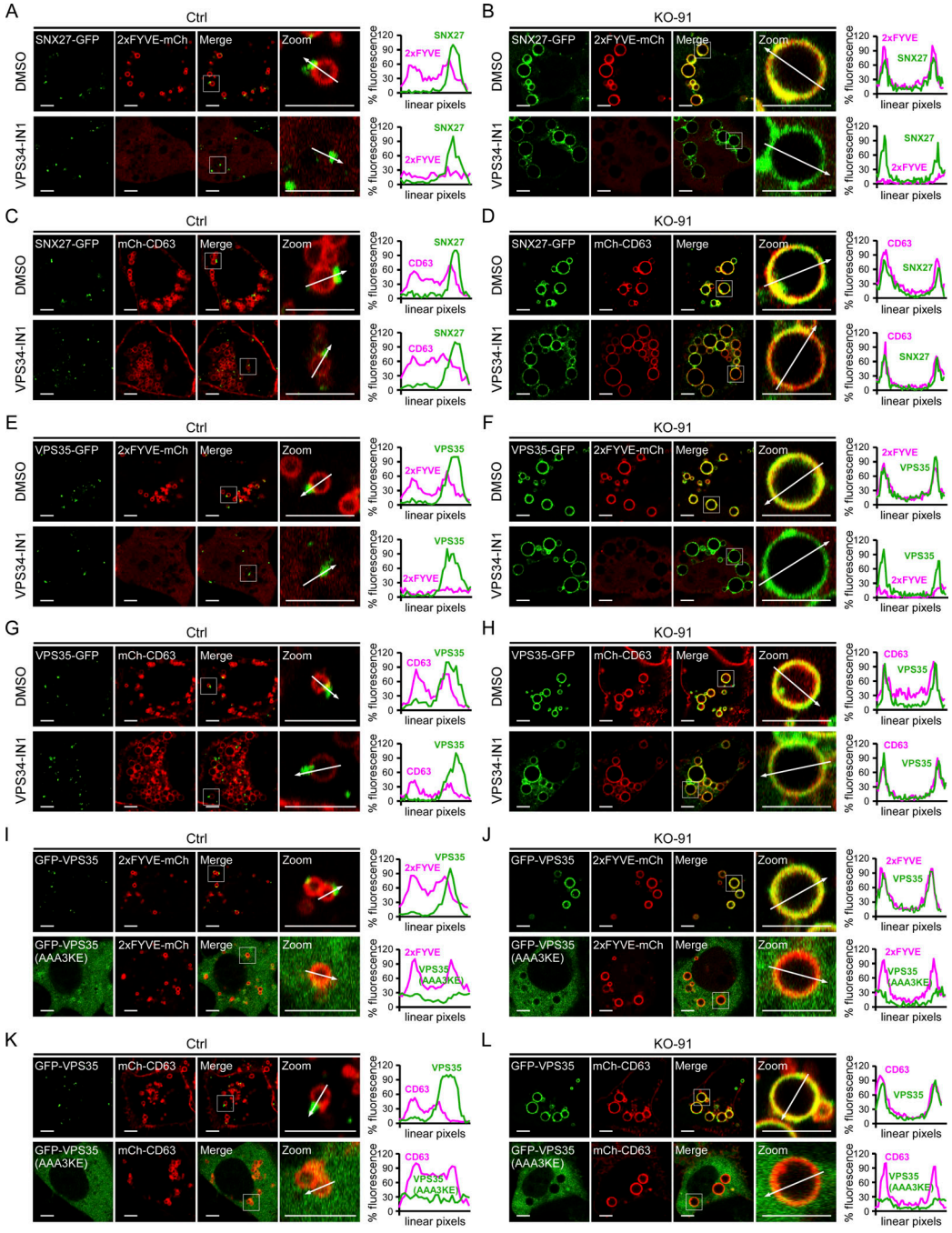

Figure S1. **Endosomal localization of GFP-tagged SNX27, VPS35, and VPS35(AAA3KE). (A and B)** Co-localization of SNX27-GFP with 2×FYVE-mCh without or with VPS34-IN1 treatment (2 µM, 3 h) in Ctrl (A) and KO-91 (B) cells. Zoom images show magnified frames in the merged images. Bars, 5 µm. Quantifications of linear pixel fluorescence of SNX27-GFP (green) and 2×FYVE-mCh (magenta) along the arrows across the endosomes in the zoom images are shown on the right. **(C and D)** Co-localization of SNX27-GFP with mCh-CD63 without or with VPS34-IN1 treatment (2 µM, 3 h) in Ctrl (C) and KO-91 (D) cells. Zoom images show magnified frames in the merged images. Bars, 5 µm. Quantifications of linear pixel fluorescence of SNX27-GFP (green) and mCh-CD63 (magenta) along the arrows across the endosomes in the zoom images are shown on the right. **(E and F)** Co-localization of VPS35-GFP with 2×FYVE-mCh without or with VPS34-IN1 treatment (2 µM, 3 h) in Ctrl (E) and KO-91 (F) cells. Zoom images show magnified frames in the merged images. Bars, 5 µm. Quantifications of linear pixel fluorescence of VPS35-GFP (green) and 2×FYVE-mCh (magenta) along the arrows across the endosomes in the zoom images are shown on the right. **(G and H)** Co-localization of VPS35-GFP with mCh-CD63 without or with VPS34-IN1 treatment (2 µM, 3 h) in Ctrl (G) and KO-91 (H) cells. Zoom images show magnified frames in the merged images. Bars, 5 µm. Quantifications of linear pixel fluorescence of VPS35-GFP (green) and mCh-CD63 (magenta) along the arrows across the endosomes in the zoom images are shown on the right. **(I and J)** Co-localization of GFP-VPS35 and GFP-VPS35(AAA3KE) with 2×FYVE-mCh in Ctrl (I) and KO-91 (J) cells. Zoom images show magnified frames in the merged images. Bars, 5 µm. Quantifications of linear pixel fluorescence of GFP-VPS35/GFP-VPS35(AAA3KE) (green) and 2×FYVE-mCh (magenta) along the arrows across the endosomes in the zoom images are shown on the right. **(K and L)** Co-localization of GFP-VPS35 and GFP-VPS35(AAA3KE) with mCh-CD63 in Ctrl (K) and KO-91 (L) cells. Zoom images show magnified frames in the merged images. Bars, 5 µm. Quantifications of linear pixel fluorescence of GFP-VPS35/GFP-VPS35(AAA3KE) (green) and mCh-CD63 (magenta) along the arrows across the endosomes in the zoom images are shown on the right.

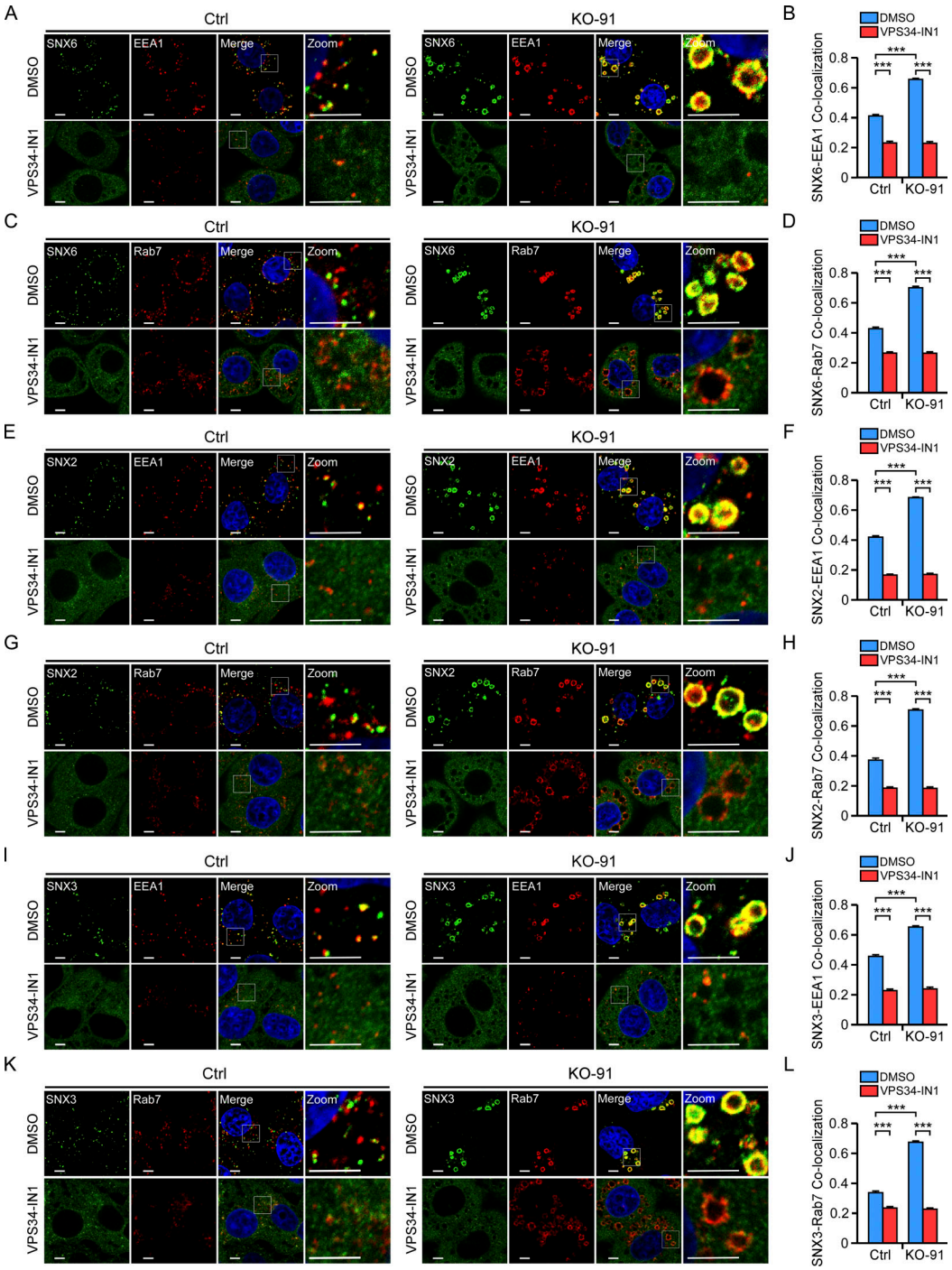

Figure S2. **Endosomal localization of SNX6, SNX2, and SNX3 depends on PtdIns3P. (A–D)** Co-localization of endogenous SNX6 with EEA1 (A and B) or Rab7 (C and D) without or with VPS34-IN1 treatment (2 µM, 3 h) in Ctrl and KO-91 cells. Zoom images show magnified frames in the merged images. Bars, 5 µm. Quantifications of SNX6-EEA1 and SNX6-Rab7 co-localization are shown in B and D. SNX6-EEA1 co-localization (B): *n* = 83 cells (Ctrl, DMSO); *n* = 70 cells (Ctrl, VPS34-IN1); *n* = 73 cells (KO-91, DMSO); *n* = 66 cells (KO-91, VPS34-IN1). SNX6-Rab7 co-localization (D): *n* = 71 cells (Ctrl, DMSO); *n* = 62 cells (Ctrl, VPS34-IN1); *n* = 61 cells (KO-91, DMSO); *n* = 74 cells (KO-91, VPS34-IN1). **(E–H)** Co-localization of endogenous SNX2 with EEA1 (E and F) or Rab7 (G and H) without or with VPS34-IN1 treatment (2 µM, 3 h) in Ctrl and KO-91 cells. Zoom images show magnified frames in the merged images. Bars, 5 µm. Quantifications of SNX2-EEA1 and SNX2-Rab7 co-localization are shown in F and H. SNX2-EEA1 co-localization (F): *n* = 53 cells (Ctrl, DMSO); *n* = 51 cells (Ctrl, VPS34-IN1); *n* = 46 cells (KO-91, DMSO); *n* = 52 cells (KO-91, VPS34-IN1). SNX2-Rab7 co-localization (H): *n* = 53 cells (Ctrl, DMSO); *n* = 49 cells (Ctrl, VPS34-IN1); *n* = 59 cells (KO-91, DMSO); *n* = 47 cells (KO-91, VPS34-IN1). **(I–L)** Co-localization of endogenous SNX3 with EEA1 (I and J) or Rab7 (K and L) without or with VPS34-IN1 treatment (2 µM, 3 h) in Ctrl and KO-91 cells. Zoom images show magnified frames in the merged images. Bars, 5 µm. Quantifications of SNX3-EEA1 and SNX3-Rab7 co-localization are shown in J and L. SNX3-EEA1 co-localization (J): *n* = 49 cells (Ctrl, DMSO); *n* = 49 cells (Ctrl, VPS34-IN1); *n* = 47 cells (KO-91, DMSO); *n* = 44 cells (KO-91, VPS34-IN1). SNX3-Rab7 co-localization (L): *n* = 51 cells (Ctrl, DMSO); *n* = 48 cells (Ctrl, VPS34-IN1); *n* = 47 cells (KO-91, DMSO); *n* = 45 cells (KO-91, VPS34-IN1). For all quantifications, the y-axis shows the value of Pearson's correlation coefficient. Error bars represent SEM. Data are from three independent experiments. Statistical analyses were performed with the Kruskal–Wallis test. ***, P < 0.001.

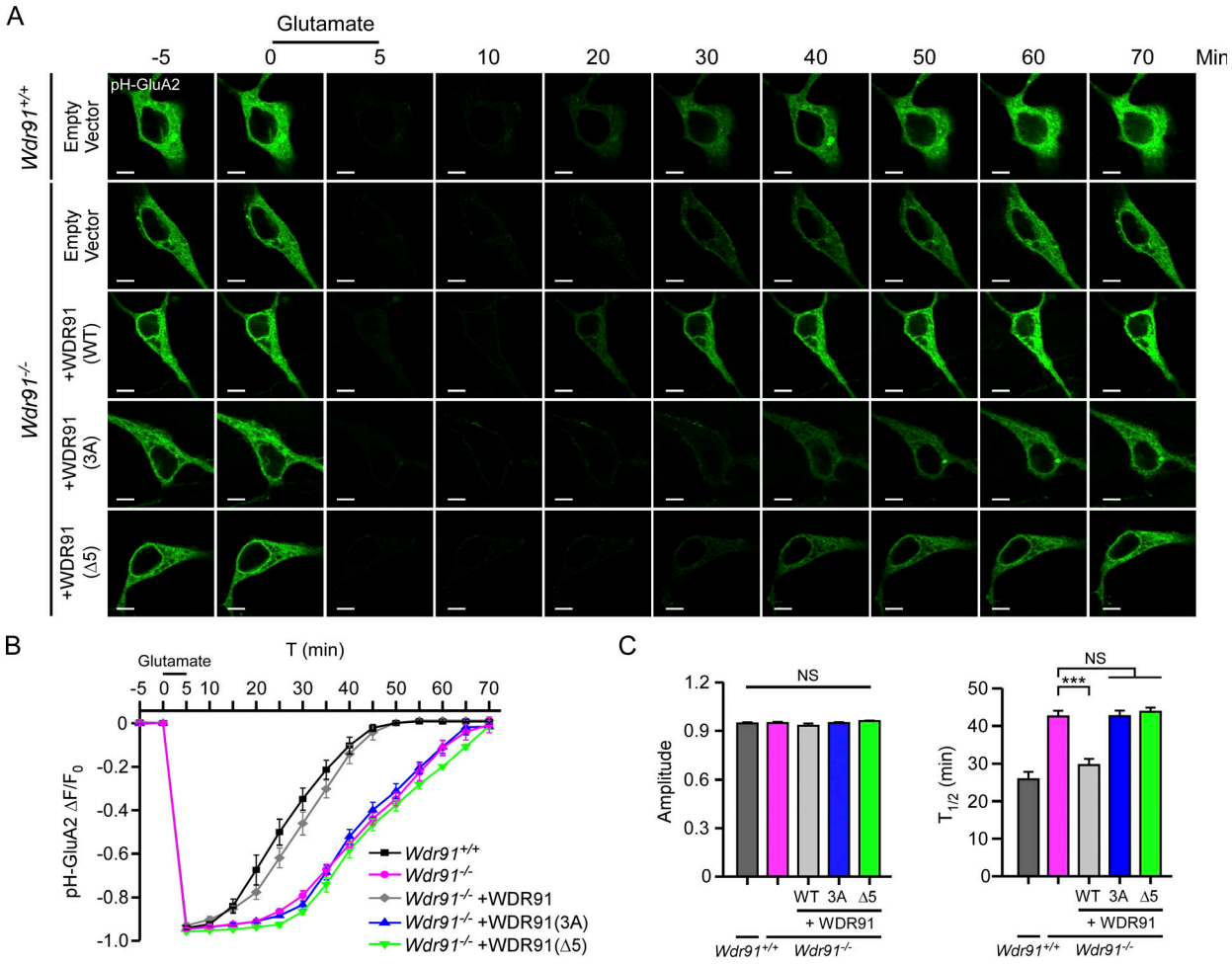

Figure S3. **Rescue of defective GluA2 recycling by Flag-WDR91, Flag-WDR91(3A), and Flag-WDR91(Δ5) in *Wdr91*$^{-/-}$ mouse primary neurons. (A)** Time-course recording of pH-GluA2 in mouse primary hippocampal neurons with the indicated genotypes. Neurons were transfected with pH-GluA2– and WDR91-expressing vectors and subjected to glutamate perfusion for 5 min. Glutamate was removed at the time point 5 min, and neurons were continuously imaged. Bars, 5 µm. **(B)** Time-course tracing of pH-GluA2 fluorescence intensity in neurons shown in A. *n* = 9 neurons (*Wdr91*$^{+/+}$); *n* = 7 neurons (*Wdr91*$^{-/-}$); *n* = 6 neurons (*Wdr91*$^{-/-}$ + WDR91[WT]); *n* = 6 neurons (*Wdr91*$^{-/-}$ + WDR91[3A]); *n* = 6 neurons (*Wdr91*$^{-/-}$ + WDR91[Δ5]). **(C)** Left: Maximum amplitudes of pH-GluA2 fluorescence intensity changes upon glutamate stimulation. Right: Average half-time ($T_{1/2}$) of pH-GluA2 fluorescence recovery after removal of glutamate. *n* = 9 neurons (*Wdr91*$^{+/+}$); *n* = 7 neurons (*Wdr91*$^{-/-}$); *n* = 6 neurons (*Wdr91*$^{-/-}$ + WDR91[WT]); *n* = 6 neurons (*Wdr91*$^{-/-}$ + WDR91[3A]); *n* = 6 neurons (*Wdr91*$^{-/-}$ + WDR91[Δ5]). For all quantifications, error bars represent SEM. Data are from three independent experiments. Statistical analyses were performed with the Kruskal–Wallis test. ***, P < 0.001. NS, P > 0.05.

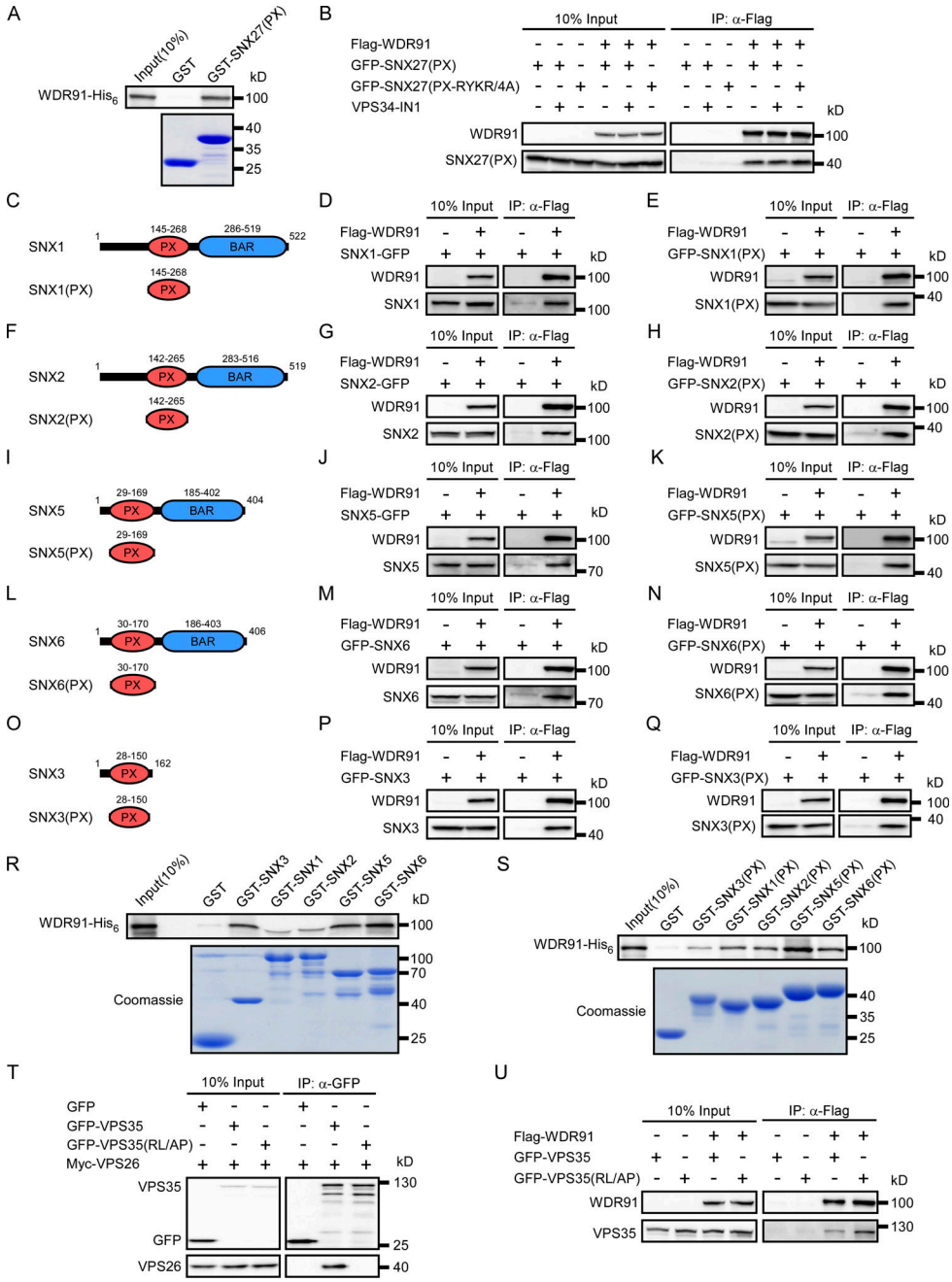

Figure S4. **Characterization of the interaction of WDR91 with retromer components. (A)** GST and GST-SNX27(PX) immobilized on glutathione-Sepharose beads were incubated with WDR91-His_6. The precipitates were immunoblotted with His_6 antibody. GST-fusion proteins were stained with Coomassie blue. **(B)** Co-IP of Flag-WDR91 with GFP-SNX27(PX) without or with VPS34-IN1 treatment, and co-IP of Flag-WDR91 with the PtdIns3P binding-deficient mutant GFP-SNX27(PX-RYKR/4A). IPs were performed with anti-Flag antibody resin and immunoblotted using Flag and GFP antibodies. **(C–E)** Co-IP of Flag-WDR91 with SNX1-GFP. Schematic representation of SNX1 is shown in C. Co-IPs of Flag-WDR91 with SNX1-GFP and GFP-SNX1(PX) are shown in D and E, respectively. **(F–H)** Co-IP of Flag-WDR91 with SNX2-GFP. Schematic representation of SNX2 is shown in F. Co-IPs of Flag-WDR91 with SNX2-GFP and GFP-SNX2(PX) are shown in G and H, respectively. **(I–K)** Co-IP of Flag-WDR91 with SNX5-GFP. Schematic representation of SNX5 is shown in I. Co-IPs of Flag-WDR91 with SNX5-GFP and GFP-SNX5(PX) are shown in J and K, respectively. **(L–N)** Co-IP of Flag-WDR91 with GFP-SNX6. Schematic representation of SNX6 is shown in L. Co-IPs of Flag-WDR91 with GFP-SNX6 and GFP-SNX6(PX) are shown in M and N, respectively. **(O–Q)** Co-IP of Flag-WDR91 with GFP-SNX3. Schematic representation of SNX3 is shown in O. Co-IPs of Flag-WDR91 with GFP-SNX3 and GFP-SNX3(PX) are shown in P and Q, respectively. **(R)** GST, GST-SNX3, and the indicated GST-SNX-BAR proteins immobilized on glutathione-Sepharose beads were incubated with WDR91-His_6. The precipitates were immunoblotted with His_6 antibody. GST-fusion proteins were stained with Coomassie blue. **(S)** GST, GST-SNX3(PX), GST-SNX1(PX), GST-SNX2(PX), GST-SNX5(PX), and GST-SNX6(PX) immobilized on glutathione-Sepharose beads were incubated with WDR91-His_6. The precipitates were immunoblotted with His_6 antibody. GST-fusion proteins were stained with Coomassie blue. **(T)** Co-IP of GFP-tagged VPS35 and VPS35 carrying the PRLYL motif mutation (GFP-VPS35[RL/AP]) with Myc-VPS26. IPs were performed with GFP-trap beads, and precipitated proteins were immunoblotted using Myc and GFP antibodies. **(U)** Co-IP of Flag-WDR91 with GFP-VPS35 or GFP-VPS35(RL/AP). IPs were performed with anti-Flag antibody resin and immunoblotted using Flag and GFP antibodies. Source data are available for this figure: SourceData FS4.

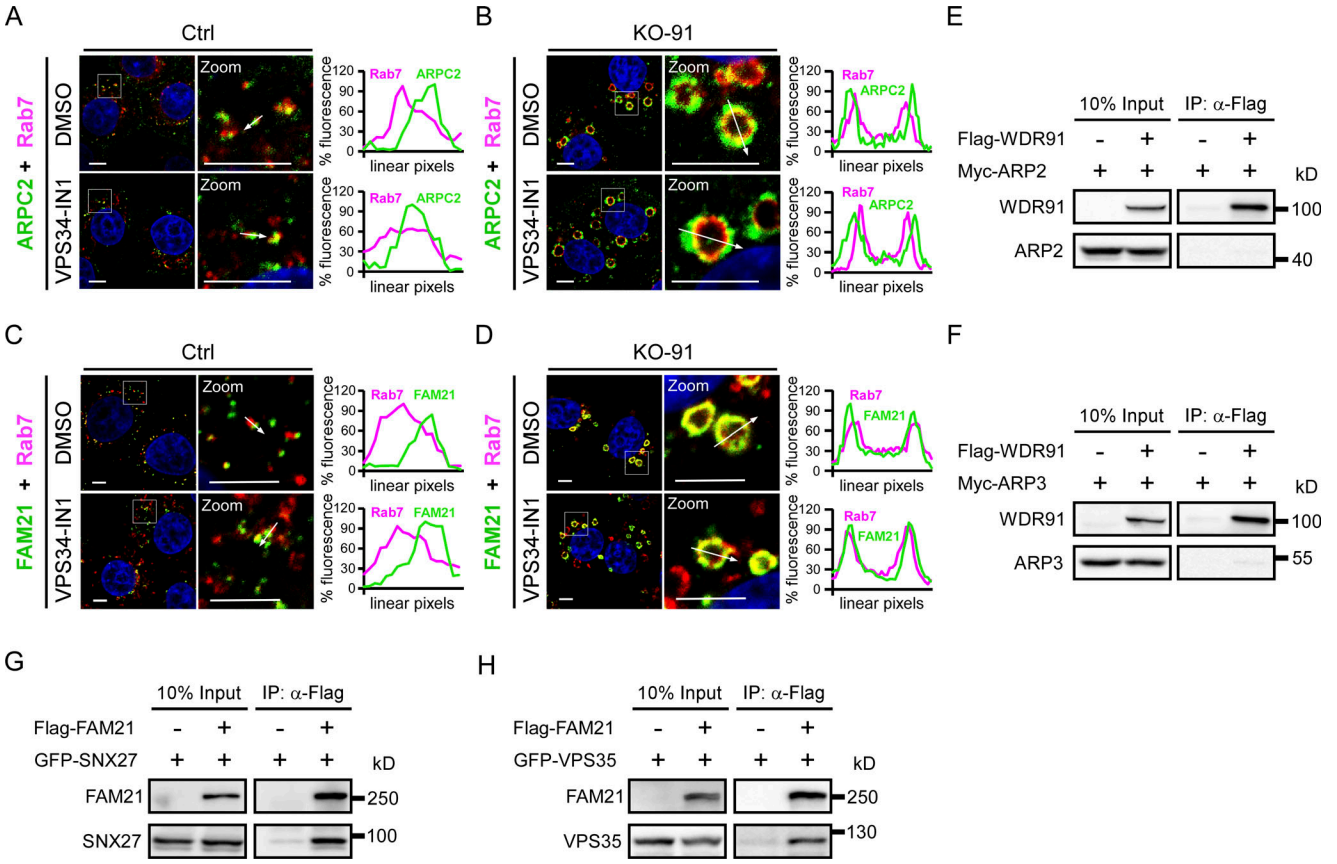

Figure S5. **Characterization of endosomal association of ARP2/3 and WASH components, and the interaction of ARP2/3 with WDR91, and FAM21 with SNX27 or VPS35. (A and B)** Co-immunostaining of endogenous ARPC2 with Rab7 in Ctrl (A) and KO-91 (B) cells treated without or with VPS34-IN1 (2 μM, 3 h). Zoom images show magnified frames in the merged images. Bars, 5 μm. Quantifications of linear pixel fluorescence along the arrows across the endosomes in the zoom images are shown on the right. Green: ARPC2; Magenta: Rab7. **(C and D)** Co-immunostaining of endogenous FAM21 with Rab7 in Ctrl (C) and KO-91 (D) cells treated without or with VPS34-IN1 (2 μM, 3 h). Zoom images show magnified frames in the merged images. Bars, 5 μm. Quantifications of linear pixel fluorescence along the arrows across the endosomes in the zoom images are shown on the right. Green: FAM21; Magenta: Rab7. **(E and F)** Co-IP of Flag-WDR91 with Myc-ARP2 (E) and Myc-ARP3 (F). IPs were performed with anti-Flag antibody resin and immunoblotted using Flag and Myc antibodies. **(G and H)** Co-IP of Flag-FAM21 with GFP-SNX27 (G) and GFP-VPS35 (H). IPs were performed with anti-Flag antibody resin and immunoblotted using Flag and GFP antibodies. Source data are available for this figure: SourceData FS5.

Video 1. **Time-lapse monitoring of SNX27-GFP on 2×FYVE-mCh-positive endosomes in Ctrl and KO-91 HeLa cells.** Related to Fig. 2 G. Ctrl and KO-91 cells co-transfected with plasmids encoding SNX27-GFP (green) and 2×FYVE-mCh (red) were imaged by time-lapse fluorescence microscopy. The frames were taken every 5 s and are displayed at 5 frames per sec (fps). Endosomal SNX27-GFP tubulation events are indicated with arrows in different colors. Bars, 2 μm.

Video 2. **Time-lapse monitoring of SNX27-GFP on mCh-CD63–positive endosomes in Ctrl and KO-91 HeLa cells.** Related to Fig. 2 I. Ctrl and KO-91 cells co-transfected with plasmids encoding SNX27-GFP (green) and mCh-CD63 (red) were imaged by time-lapse fluorescence microscopy. The frames were taken every 5 s and are displayed at 5 fps. Endosomal SNX27-GFP tubulation events are indicated with arrows in different colors. Bars, 2 μm.

Video 3. **Time-lapse monitoring of SNX27-GFP and mCh-WDR91 in HeLa cells.** Related to Fig. 6 K. HeLa cells co-transfected with plasmids encoding SNX27-GFP (green) and mCh-WDR91 (red) were imaged by time-lapse fluorescence microscopy. The frames were taken every 5 s and are displayed at 5 fps. Tubulation of SNX27-GFP at mCh-WDR91–enriched sites is indicated by arrows. Bars, 2 μm.

Video 4. **Time-lapse monitoring of VPS35-GFP and mCh-WDR91 in HeLa cells.** Related to Fig. 6 L. HeLa cells co-transfected with plasmids encoding VPS35-GFP (green) and mCh-WDR91 (red) were imaged by time-lapse fluorescence microscopy. The frames were taken every 5 s and are displayed at 5 fps. Tubulation of VPS35-GFP at mCh-WDR91–enriched sites is indicated by arrows. Bars, 2 µm.

Provided online are two tables. Table S1 lists the commercial antibodies and reagents used in the study. Table S2 lists the expression vectors used in the study.